





ARTICLE

Pluripotency exit is guided by the *Peln1*-mediated disruption of intrachromosomal architecture

Yichen Wang^{1,2,3*}, Lin Jia^{1,3*}, Cong Wang^{1,3}, Zhonghua Du³, Shilin Zhang^{1,3}, Lei Zhou^{1,3}, Xue Wen², Hui Li², Huiling Chen³, Yuanyuan Nie^{1,3}, Dan Li¹, Shanshan Liu^{1,3}, Daniela Salgado Figueroa⁴, Ferhat Ay⁴, Wei Xu¹, Songling Zhang¹, Wei Li¹, Jiuwei Cui^{1**}, Andrew R. Hoffman^{2**}, Hui Guo^{2**}, and Ji-Fan Hu^{1,3**}

The molecular circuitry that causes stem cells to exit from pluripotency remains largely uncharacterized. Using chromatin RNA in situ reverse transcription sequencing, we identified *Peln1* as a novel chromatin RNA component in the promoter complex of *Oct4*, a stem cell master transcription factor gene. *Peln1* was negatively associated with pluripotent status during somatic reprogramming. *Peln1* overexpression caused E14 cells to exit from pluripotency, while *Peln1* downregulation induced robust reprogramming. Mechanistically, we discovered that *Peln1* interacted with the *Oct4* promoter and recruited the DNA methyltransferase DNMT3A. By de novo altering the epigenotype in the *Oct4* promoter, *Peln1* dismantled the intrachromosomal loop that is required for the maintenance of pluripotency. Using RNA reverse transcription-associated trap sequencing, we showed that *Peln1* targets multiple pathway genes that are associated with stem cell self-renewal. These findings demonstrate that *Peln1* can act as a new epigenetic player and use a trans mechanism to induce an exit from the pluripotent state in stem cells.

Introduction

Pluripotent stem cells may become useful reagents in regenerative medicine and cell replacement therapy, primarily due to their indefinite self-renewal properties in vitro and their ability to differentiate into any cell type that is needed (Silva et al., 2019; Yilmaz and Benvenisty, 2019). Pluripotency is precisely regulated by a network of key transcription factor genes, including *Oct4*, *Nanog*, and *Sox2*, as well as signaling pathways, including the Wnt/ β -catenin pathway, leukemia inhibitory factor (LIF)/Janus kinase-signal transducer and activator of transcription 3 pathway, phosphoinositide 3 kinase pathway, and Ras/MAPK pathway (Ramazzotti et al., 2019; Rasmussen et al., 2018). Together, this gene regulation network orchestrates molecular processes that ensure the maintenance of pluripotent identity in stem cells. Disruption of this network leads to loss of pluripotency and cellular differentiation (Li and Izpisua Belmonte, 2018; Niwa, 2018). Understanding the molecular mechanisms required for stem cells to maintain a delicate balance between pluripotency and differentiation is critical for advancing stem cell-based therapies to clinical applications.

Mouse embryonic stem cells (ESCs) exist in naive and primed states with distinct transcriptional regulatory networks, epigenotypes, and signaling requirements (Nichols and Smith, 2009; Shiozawa et al., 2020; Weinberger et al., 2016). Mouse ESCs derived from the inner cell mass of blastocysts are considered as being in the naive state. While maintained in a self-renewing state through the LIF and BMP pathways, these cells have the ability to differentiate to produce chimeric animals. In contrast, postimplantation epiblast-derived mouse epiblast stem cells are in a primed pluripotent state; these cells are dependent on the FGF-Activin pathways and rarely form chimera. However, primed cells can be reverted to naive status by KLF4, MYC, or *Nanog* in the presence of LIF. Conversely, naive ESCs can be induced into the primed state by activating the FGF2/Activin pathway. Furthermore, naive mESCs can become homogeneous “ground-state” pluripotent stem cells under the influence of two small-molecule MEK/ERK and GSK inhibitors plus LIF (2i/LIF; Panepucci and de Souza Lima, 2019; Papp and Plath, 2011; Papp and Plath, 2013; Shiozawa et al., 2020). Despite the fact that a

¹Key Laboratory of Organ Regeneration and Transplantation of Ministry of Education, Cancer Center, First Hospital of Jilin University, Changchun, Jilin, China; ²Department of Endocrinology, First Hospital of Jilin University, Changchun, Jilin, China; ³Stanford University Medical School, VA Palo Alto Health Care System, Palo Alto, CA; ⁴La Jolla Institute for Allergy and Immunology, La Jolla, CA.

*Y. Wang and L. Jia contributed equally to the paper. Correspondence to Ji-Fan Hu: jifan@stanford.edu or hujifan@jlu.edu.cn; Hui Guo: ghui@jlu.edu.cn; Jiuwei Cui: cuijw@jlu.edu.cn; Andrew R. Hoffman: arhoffman@stanford.edu

**Jiuwei Cui, Andrew R. Hoffman, Hui Guo, and Ji-Fan Hu are senior authors to the work.

© 2022 Wang et al. This article is distributed under the terms of an Attribution–Noncommercial–Share Alike–No Mirror Sites license for the first six months after the publication date (see <http://www.rupress.org/terms/>). After six months it is available under a Creative Commons License (Attribution–Noncommercial–Share Alike 4.0 International license, as described at <https://creativecommons.org/licenses/by-nc-sa/4.0/>).

number of pathways are known to be involved in the inter-conversion of these states, specific underlying mechanisms remain to be characterized.

Stem cell fate is dynamically regulated by balanced self-renewal and differentiation signals. To initiate the exit from pluripotency toward differentiation, cells need to disable pluripotency-specific transcriptional networks and activate lineage-specific pathways (Betschinger et al., 2013; Kalkan and Smith, 2014). In response to differentiation signals, such as withdrawal of LIF from the culture medium or treatment with retinoic acid, pluripotent stem cells dismantle the naive pluripotency network and shut down the expression of the stem cell core transcription factors. The molecular components that coordinate pluripotent exit are poorly understood.

Long noncoding RNAs (lncRNAs) have versatile biological functions in a variety of biological processes (Huang et al., 2019; Jae et al., 2019; Kopp, 2019; Krishnan and Mishra, 2014). Recent studies suggest that lncRNAs may play important roles in regulating the network that contributes to ESC self-renewal and differentiation (Fico et al., 2019; Mirzadeh Azad et al., 2021; Perry and Ulitsky, 2016). Multiple pluripotency-associated lncRNAs have been identified embedded in the chromatin regulatory network using CRISPR Cas9 screening, RNA transcriptome sequencing (RNA-seq), and RNA reverse transcription-associated trap sequencing (RAT-seq; Chen et al., 2019; Chen et al., 2020; Du et al., 2018; Zhu et al., 2020b). These lncRNAs regulate the pluripotency network using a variety of epigenetic mechanisms. After binding to pluripotency-associated gene promoters, like *Oct4* and *Sox2*, these lncRNAs coordinate the construction of a pluripotency-specific intrachromosomal loop, modulate promoter methylation by recruiting demethylase TET1, and activate the eRNA pathway of stemness genes (Cao et al., 2021; Du et al., 2021; Zhu et al., 2020a).

However, little information is available about the role of lncRNAs in controlling the exit of stem cells from the pluripotent status. To better understand the underlying mechanisms leading to pluripotent exit and initiation of lineage specification, we explored a novel strategy to identify lncRNAs that interact with the promoter of *Oct4*, a master transcription factor that maintains the ground pluripotent state. By using chromatin RNA in situ reverse transcription sequencing (CRIST-seq; Zhang et al., 2019), we identified *Peln1* as an important lncRNA component in the circuitry that controls the exit from pluripotency in stem cells. Notably, we showed that *Peln1* exerted this function by regulating the activity of the *Oct4* promoter in trans. These findings may shed light on our understanding of the molecular basis of lncRNAs as new chromatin players in the regulatory network of stem cells.

Results

Identification of *Peln1* as a lncRNA associated with exit from pluripotency

We used a novel strategy to map functional lncRNAs related to pluripotency exit in stem cells (Fig. 1 A). First, a CRIST-seq approach (Zhang et al., 2019) was used to identify functional lncRNAs that interact with the promoter of *Oct4*, a critical master

factor that is required for the maintenance of stem cell pluripotency (Fig. S1 A). Un-reprogrammed fibroblasts were used for the initial CRIST-seq screening of lncRNAs that negatively regulate *Oct4*. Cells were transfected to express a lentiviral dCas9 *Oct4* gRNA cassette. After membrane lysis, the nuclei were collected and RNAs were reverse transcribed in situ with biotin-dCTP. The *Oct4*-lncRNA-cDNA chromatin complex was pulled down by Cas9-FLAG immunoprecipitation. The biotin-cDNA complexes were then purified with streptavidin beads. Using quantitative PCR (Q-PCR), we showed that the *Oct4* gRNA guided Cas9 specifically to the targeting site (Site I) at the *Oct4* locus. There was a very low binding signal at the control site (Site II). Only slight background signals were detected in the vector control (Vector) and the Cas9 random gRNA control (gCT; Fig. S1 B). After confirming specific Cas9 *Oct4* gRNA targeting, the CRIST library was constructed for Illumina sequencing (Zhang et al., 2019).

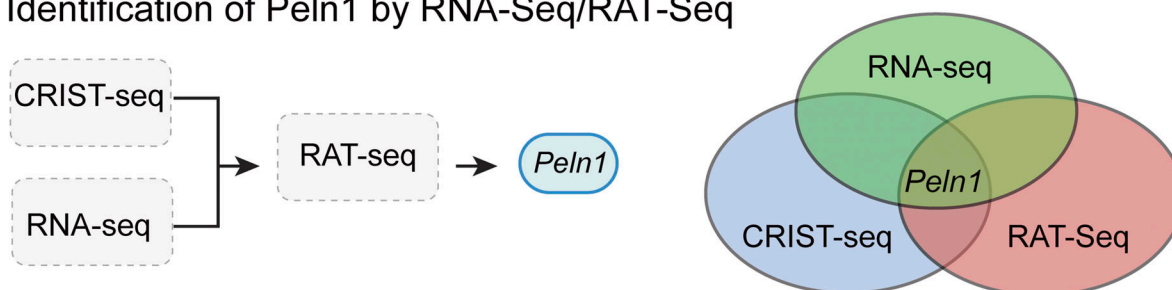
Conventional RNA-seq was performed to identify differentially expressed lncRNAs related to the induction of pluripotent stem cells (Du et al., 2018). The RNA-seq dataset was then integrated with the CRIST-seq dataset to identify potential lncRNAs that are not only silenced during pluripotency induction, but also have the ability to regulate the *Oct4* gene (Fig. 1 A).

Using this strategy, we identified lncRNA NONMMUT056388 as a novel RNA molecule that is associated with exit from pluripotency in stem cells. We refer to this lncRNA as *Peln1* (pluripotency exit lncRNA 1). Quantitative CRIST-PCR confirmed that *Peln1* was enriched in the Cas9 *Oct4* gRNA library, but not in the Cas9 vector control and Cas9 random gRNA (gCT) libraries (Fig. S1 C). The other two control lncRNAs, *Prdl4* and *Prdl5* (pluripotent reprogramming-downregulated lncRNA 4, 5) were not detected in the *Oct4* promoter complex. The RNA-seq data indicated that *Peln1* was expressed in fibroblasts but was silenced when cells completed reprogramming into iPSCs.

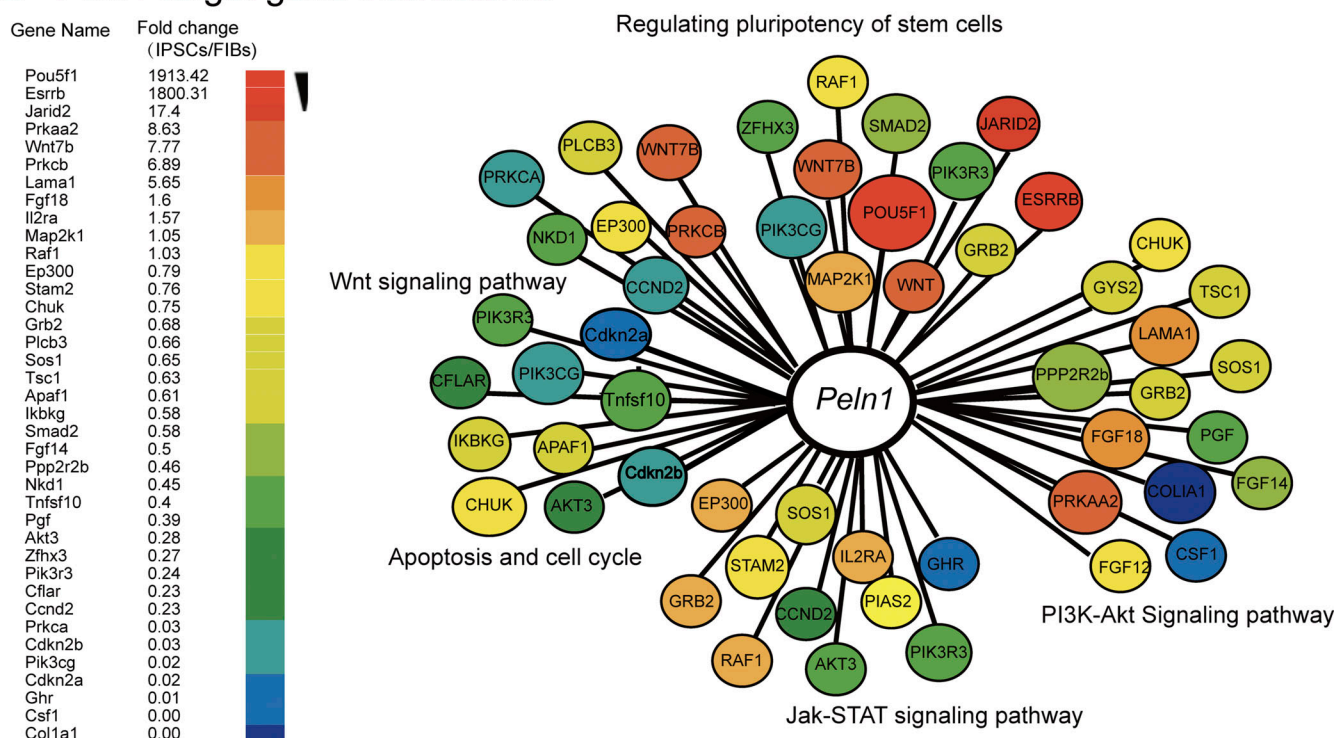
Finally, we used RAT-seq to identify the genome-wide interaction targets for *Peln1* (Fig. S1 D; Chen et al., 2018; Sun et al., 2014; Wang et al., 2014). Cells were cross-linked to fix the lncRNA-chromatin structure, and chromatin RNAs were reverse transcribed in situ using three *Peln1*-specific complementary primers (Table S1) containing biotin-dCTP. The *Peln1* cDNA-interacting chromatin complex was pulled down with streptavidin beads and the target gene DNAs were purified for library sequencing. A control RAT library was constructed using random oligonucleotide primers. The *Peln1* RAT-seq data were normalized over the peaks of the control RAT-seq data to map the lncRNA target gene interaction network. Using RAT-seq analysis, we found that *Peln1* interacted with numerous pluripotency-associated genes (Fig. 1 B). Specifically, *Peln1* interacted with the promoter and enhancer of the stem cell core factor *Oct4* (Fig. 1 C) and the regulatory elements of *Sox2* and *Nanog* (Fig. S1, E and F).

We then characterized the gene structure of *Peln1*. Using 5'-rapid amplification of cDNA ends (RACE) and 3'-RACE, we obtained the full-length cDNA for *Peln1* (Fig. S2, A-D). We also cloned the 2 kb upstream fragment of *Peln1* as its putative promoter and inserted it into the pGL3 vector to generate a luciferase reporter construct (Fig. S2 E). The luciferase reporter assay showed that this 2 kb upstream fragment contained strong promoter activity. These data suggest that *Peln1* may be transcribed

A Identification of *Peln1* by RNA-Seq/RAT-Seq



B *Peln1* target gene interactome



C *Peln1* binds to the *Oct4* locus

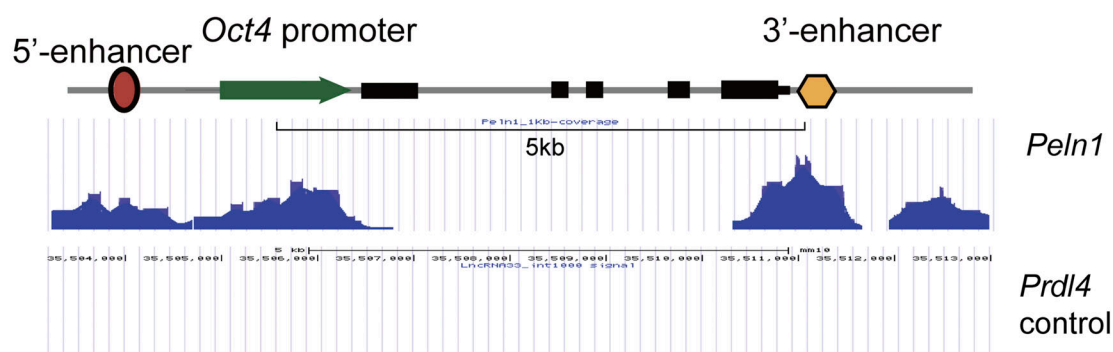


Figure 1. Identification of pluripotency-associated lncRNA *Peln1* by RNA-seq, CRIST-seq, and RAT-seq. (A) Identification of the pluripotency-associated lncRNA *Peln1* by integrating RNA-seq, CRIST-seq, and RAT-seq. CRIST-seq: chromatin RNA in situ reverse transcription sequencing, which was used to identify the *Oct4* promoter-interacting lncRNAs in fibroblasts; RNA-seq: transcriptome sequencing to identify the differentially expressed lncRNAs between fibroblasts and iPSCs; RAT-seq: RNA reverse transcription-associated trap sequencing, which was used to profile the genome-wide target genes for the identified lncRNAs. By integrating these datasets, we identified *Peln1* as a pluripotency-associated lncRNA used for further studies. (B) *Peln1* interaction network targets identified by RAT-seq. *Peln1* binds to pathway genes that are involved in stem cell development, cell fate, and signaling pathways. Target genes with fold-enrichment >10 were chosen from *Peln1* RAT-seq and were integrated with differentially expressed genes from the iPSC-fibroblast RNA-seq data. Target genes were sorted from high to low based on the fold-change of iPSCs/fibroblasts. (C) Binding signal of *Peln1* lncRNA in the *Oct4* locus. *Prdl4* was used as the lncRNA control.

from an intergenic promoter that is located in the *Ptn* (Pleiotrophin) gene locus.

We also examined whether the status of DNA methylation in the *Pelnl* promoter was related to differential expression of *Pelnl* between fibroblasts and E14 cells. We found that one of the CpGs was completely unmethylated in E14 cells but was completely methylated in fibroblasts and mouse embryonic fibroblasts (MEFs; Fig. S2 F), suggesting that the *Pelnl* promoter may be regulated by transcriptional repressors that bind to the unmethylated CpG sites.

***Pelnl* is negatively associated with stem cell pluripotency**

We then conducted a series of assays to characterize the role of *Pelnl* in stem cells. We first quantitated the expression of *Pelnl* during pluripotent reprogramming, showing that the expression of *Pelnl* was negatively correlated with pluripotency. *Pelnl* was highly expressed in fibroblasts as well as un-reprogrammed cells (non-iPSCs), which expressed four viral reprogramming factors (OSKM), but failed to complete reprogramming (Zhang et al., 2013). However, *Pelnl* became silenced once cells were fully reprogrammed into iPSCs (Fig. 2 A). The gene was also silenced in embryonic stem cells (E14). Q-PCR confirmed that *Pelnl* was highly expressed in fibroblasts and non-iPSCs (Fig. 2 B) and expressed at variable levels in adult tissues (Fig. S2 G). *Pelnl* was upregulated in E14 cells after LIF withdrawal (Fig. S2 H), but there was little difference in *Pelnl* expression between the cultured “primed” cells and “naive” cells (Fig. S2 I).

The cytoplasmic and nuclear fraction assay showed that *Pelnl* was predominantly located in the nucleus (Fig. 2 C). RNA-FISH confirmed the nuclear localization (Fig. 2 D). During embryoid body differentiation, *Pelnl* was activated in parallel with decreased expression of *Oct4*, *Sox2*, and *Nanog* (Fig. 2 E). These data suggest that *Pelnl* is a critical nuclear factor that is negatively associated with stem cell pluripotency.

***Pelnl* promotes exit from pluripotency in E14 cells**

To examine the function of *Pelnl* in pluripotency, we cloned the full length of *Pelnl* cDNA into a lentiviral expression vector and overexpressed it in E14 cells. The empty lentiviral vector was used as a negative control (Fig. S3 A). The success of lentiviral transfection was tracked using the DsRed fluorescence marker in the lentiviral vector. After partial puromycin selection, *Pelnl*-expressing E14 cells (red) showed obvious morphological changes and lost the stem cell marker OCT4 (Fig. 3 A, top panel, red arrows). In those cells that did not express *Pelnl*, OCT4 was detected by immunostaining, suggesting that the untargeted cells remained pluripotent. After complete puromycin selection, all E14 cells became differentiated (middle panel). As expected, normal cell morphology and the stem cell marker OCT4 were preserved in the vector control cells that expressed the DsRed tracking maker (bottom panel).

We also collected DsRed-expressing cells and used Q-PCR to measure the expression of the stem cell core factor genes *Oct4*, *Sox2*, and *Nanog*. As compared with the vector control and the untreated cells, cells that overexpressed *Pelnl* had decreased expression of these three pluripotent-associated factor genes (Fig. 3 B). We also quantitated three lineage markers in these

cells and found that they expressed relatively high markers in the endoderm lineage (Fig. 3 C). The colony formation assay also showed reduced self-renewal capacity in *Pelnl*-overexpressing E14 cells (Fig. S3 B).

Pelnl knockdown enhances reprogramming

Since *Pelnl* is negatively associated with stem cell pluripotency, we examined whether knockdown of *Pelnl* was able to enhance pluripotent reprogramming. Four *Pelnl* shRNAs (shRNA-1, shRNA-2, shRNA-3, and shRNA-4) were cloned into two separate lentiviral vectors (shPelnl-1 and shPelnl-2; Fig. S3 C). The pGreenPuro *Pelnl*-shRNA lentiviruses were transduced into MEFs that carried the doxycycline (DOX)-inducible *Oct4*-*Sox2*-*Klf4*-c-Myc (Carey et al., 2010). Two control lentiviral groups were used in parallel with the shPelnl group, including a mock virus that carries the empty vector (Vector) and the control virus that carries random shRNAs (shCT). The copGFP reporter gene in the lentiviral vector was used as the green fluorescence tracking marker for lentiviral infection.

After lentiviral transfection, MEFs were selected by puromycin. Pluripotency was induced by the addition of the reprogramming inducer DOX. On day 12 of reprogramming, iPSC colonies started to form. The efficiency of iPSC colony formation was assessed by immunostaining of the pluripotency biomarker NANOG (Fig. 4 A, red). After *Pelnl* knockdown (Fig. 4 B), we observed significant increase in the number of NANOG-positive colonies as compared with the two control groups (Fig. 4 C). On day 3 after lentiviral infection, cells were collected to confirm the *Pelnl* knockdown by Q-PCR. *Pelnl* knockdown was accompanied with the upregulation of the stem cell core factors *Oct4*, *Sox2*, and *Nanog* (Fig. 4 D). These data suggest that downregulation of *Pelnl* increases the efficiency of pluripotent reprogramming. However, downregulation of *Pelnl* alone was not sufficient to induce reprogramming in fibroblasts. The OSKM cocktail factors were still needed to initiate the pluripotency.

***Pelnl* binds to Oct4 and coordinates intrachromosomal looping**

To gain insights into the mechanistic basis for *Pelnl* action, we focused on the lncRNA-mediated regulation of the *Oct4* gene, one of the most important factors in the maintenance of the pluripotent state. Since *Pelnl* interacts with the *Oct4* locus, we used Q-PCR to quantitate the *Pelnl* interaction using primers covering the whole *Oct4* locus, including the promoter (sites E-F) and enhancers (sites A-B and sites M-N; Fig. 5 A, top panel). *Pelnl* primarily interacted with the *Oct4* promoter and enhancer at E-F and M-N sites (bottom panel). Relatively few abundant background interaction signals were detected in the random control RAT group (Ctl).

Previous work has demonstrated the importance of specific intrachromosomal enhancer-promoter architecture for activation of endogenous pluripotency genes during reprogramming (Zhang et al., 2013). As *Pelnl* binds to the *Oct4* promoter and the 3'-enhancer, we hypothesized that this lncRNA might function by altering this intrachromosomal structure. We used chromatin conformation capture (3C; Dekker et al., 2002) to assess intrachromosomal looping. E14 cells were transfected

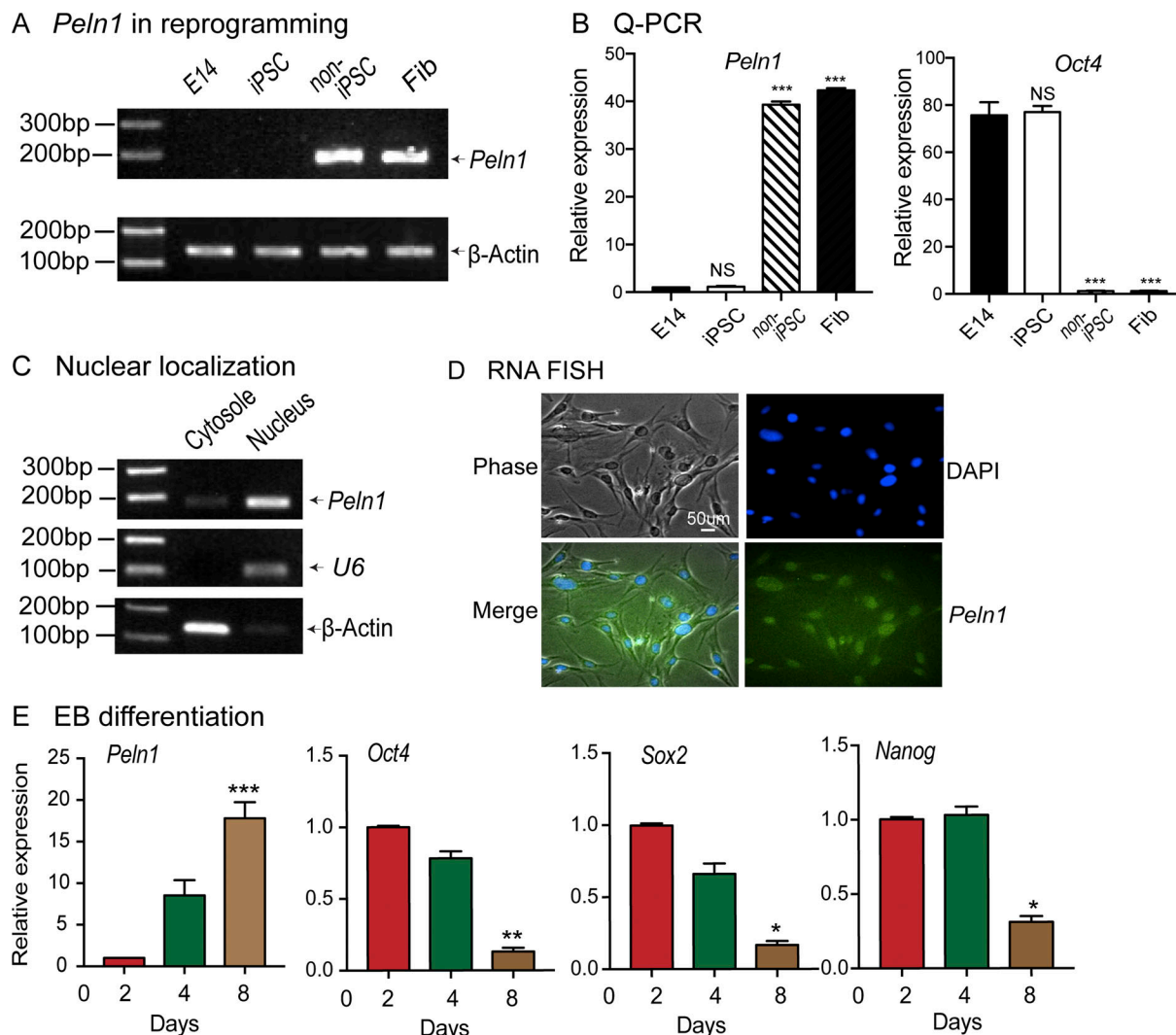


Figure 2. *Peln1* is negatively associated with stem cell pluripotency. (A) *Peln1* is negatively associated with reprogramming. MEFs were reprogrammed by DOX-inducible OSKM (*Oct4*, *Sox2*, *Klf4*, and *c-Myc*). Cells were collected at different stages of reprogramming and the expression of *Peln1* was measured by RT-PCR. Fib: fibroblasts; non-iPSC: cells that ectopically express four OSKM factors but failed to completely reprogram into pluripotency; iPSC: induced pluripotent stem cells; E14: mouse embryonic pluripotent stem cell line used as a positive control. β -Actin was used as the PCR control. (B) Q-PCR of *Peln1* in reprogramming. The data were analyzed with two-sided Student's *t* test. Data are presented as mean \pm SD of three independent experiments. ***, $P < 0.001$; NS, not significant as compared with E14 cells. (C) Nuclear localization of *Peln1*. Cytoplasmic and nuclear RNAs were isolated and used to quantitate the cellular distribution of *Peln1* lncRNA. Nuclear *U6* was used as the nuclear positive control. β -Actin was used as the cytoplasmic control. (D) *Peln1* RNA FISH. Scale bar, 50 μ m. Note the nuclear localization of *Peln1* lncRNA. (E) Expression of *Peln1* in embryoid body differentiation of E14 cells. Cells were collected at different stages of EB formation for Q-PCR. For comparison, the expression of three stem cell core factors was also quantitated. Data are presented as mean \pm SD of three independent experiments. ***, $P < 0.001$; **, $P < 0.01$; *, $P < 0.05$ compared with Day 2. Note the negative association between *Peln1* and three stem cell factors.

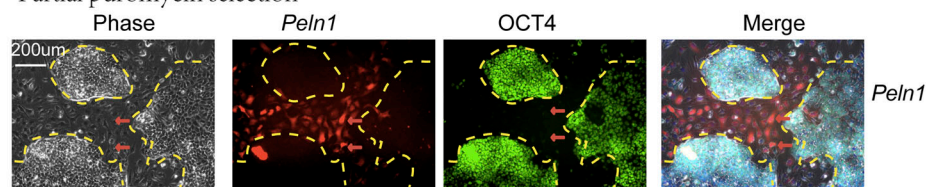
with full-length *Peln1*. The empty vector served as the mock control. The interacting chromatin complex DNAs were detected by Q-PCR using the 3C primers located in the promoter and the enhancers of *Oct4* (Fig. 5 B, top panel). We detected five intrachromosomal interaction products in untreated E14 cells and mock-treated E14 cells: JH4782/JH4783, JH4780/JH4783, JH4780/JH4785, JH4785/JH4794, and JH4788/JH4785. Overexpression of *Peln1* abolished the intrachromosomal interaction signals at three sites (bottom panel), in parallel with the exit of E14 cells from pluripotency. We sequenced the 3C products and confirmed the presence of the ligated MboI sites, flanked by the sequences from the promoter and enhancers of *Oct4* (Fig. 5 C).

These data suggest that, after binding to the regulatory elements of *Oct4*, *Peln1* abolished these vital intrachromosomal interactions, leading to exit from pluripotency.

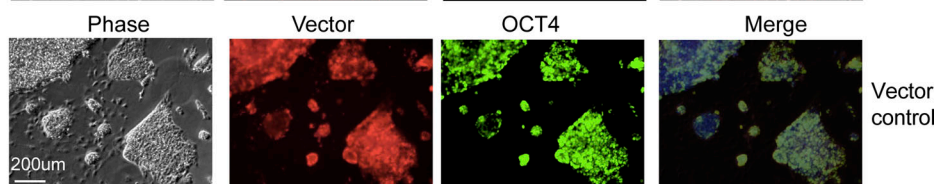
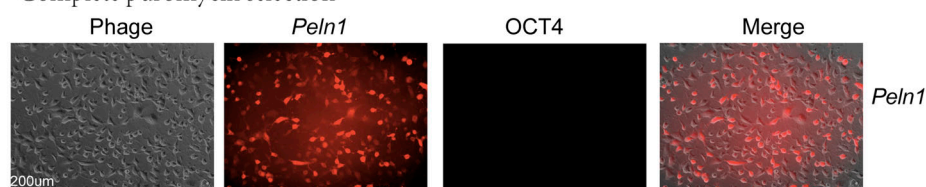
To further delineate the role of *Peln1* in this abrogation of intrachromosomal looping, we examined the Hoogsteen base-pairing binding between the *Peln1* lncRNA and the *Oct4* DNA. The lncRNA-DNA interaction prediction indicated that nearly all the predicted *Peln1*-*Oct4* base-pairing binding sites (TFO1-TFO10) were aggregated in a short fragment of the 5'-*Peln1* (Fig. S3 E). We deleted a 95 bp fragment containing the putative base-pairing region. Interestingly, the base-pairing fragment-deficient mutant lost its role in the regulation of stemness (Fig. S3 F),

A *PeIn1* induces pluripotency exit

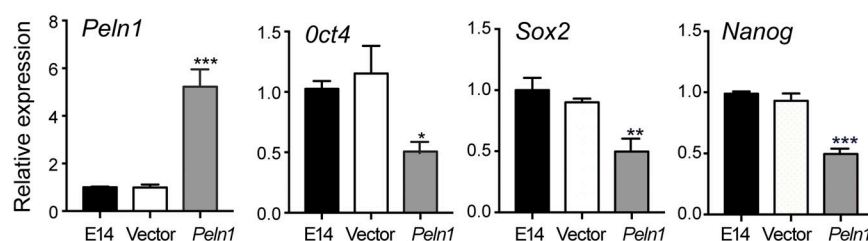
Partial puromycin selection



Complete puromycin selection



B Stem cell core factors



C Embryoid body differentiation

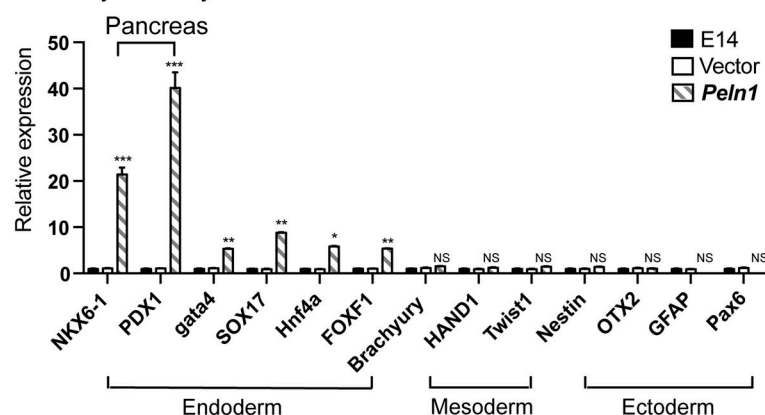
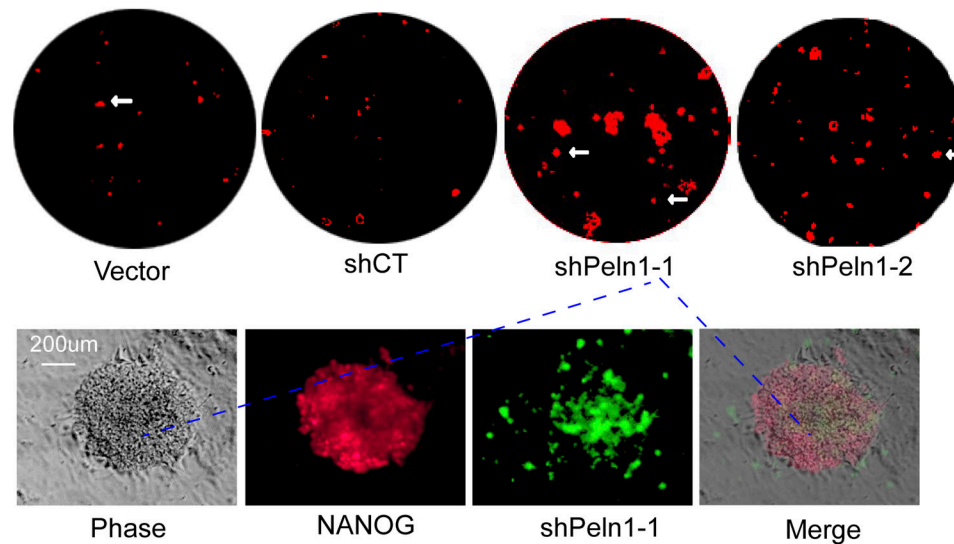
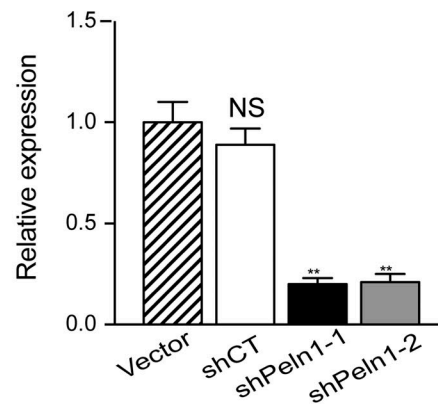
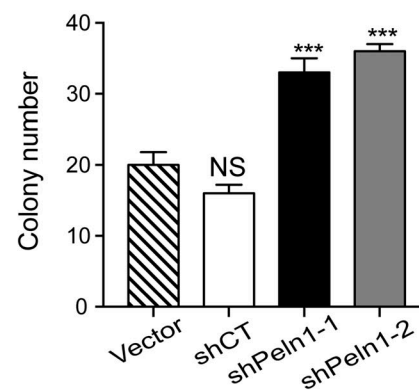


Figure 3. ***PeIn1* promotes the exit from pluripotency in E14 cells.** (A) Pluripotency staining of E14 cells. After lentiviral *PeIn1* infection, cells were partially (top panel) and completely (middle panel) selected by puromycin. Pluripotency was examined by immunohistochemical staining of the pluripotent marker OCT4 (green). Note the loss of pluripotency in *PeIn1*-expressing cells (RsRed positive). (B) Q-PCR quantitation of stem cell core factors. After *PeIn1* was overexpressed in E14 cells, stem cell core factors were detected by Q-PCR. Data are presented as mean \pm SD of three independent experiments. ***, $P < 0.001$; **, $P < 0.01$; *, $P < 0.05$ as compared with the Vector control group. (C) Role of *PeIn1* in the expression of developmental marker genes of three germ layers. After *PeIn1* was overexpressed in E14 cells, the cells were collected for the measurement of three germ layer marker genes using Q-PCR. Lentiviral vector and untreated E14 cells were used as controls. The data are presented as mean \pm SD of three independent experiments. ***, $P < 0.001$; **, $P < 0.01$; *, $P < 0.05$; NS, not significant as compared with the Vector control group. Note the significant upregulation of endodermal makers in *PeIn1*-overexpressing E14 cells.

A *Pel*1 knockdown enhances reprogrammingB *Pel*1 knockdown

C Quantitation of iPSC colonies



D Stem cell core factors

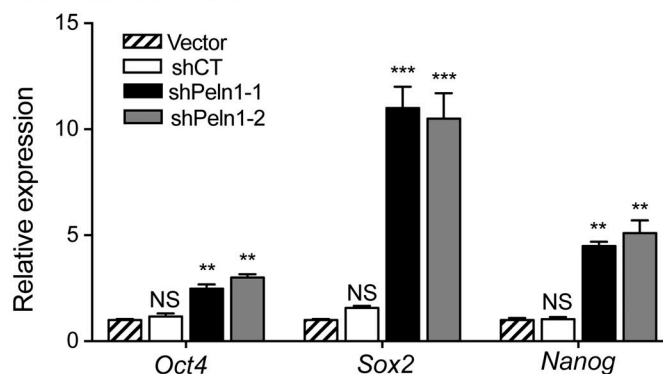
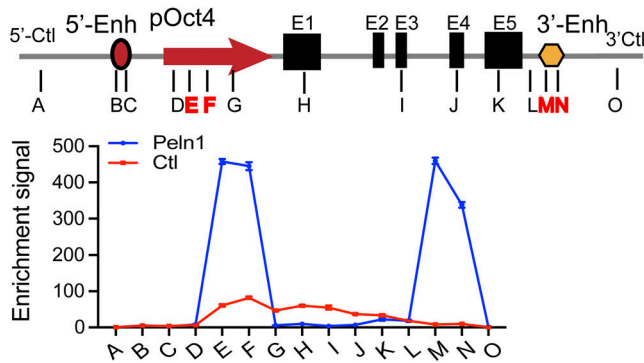
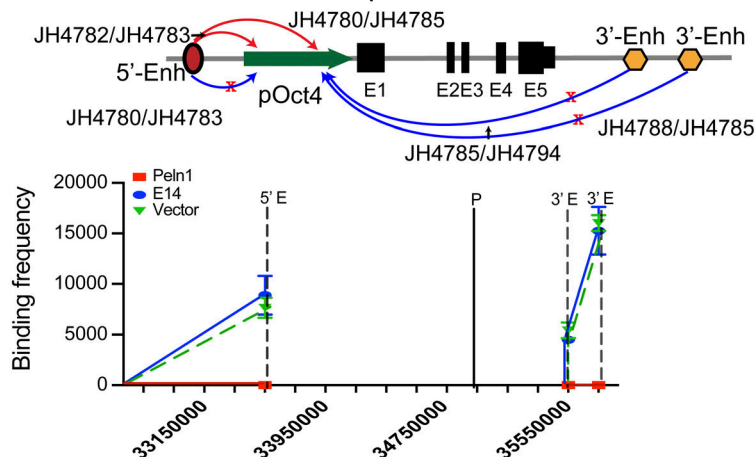


Figure 4. *Pel*1 knockdown enhances reprogramming. (A) Reprogramming efficiency is increased in the *Pel*1-deficient cells. DOX-OSKM (*Oct*4, *Sox*2, *Klf*4, and *c-Myc*) inducible MEFs were transfected with the *Pel*1 shRNA lentivirus. The random shRNA (gCT) lentivirus and the empty vector (Vector) lentivirus were used as the study controls. After lentiviral transfection, reprogramming was induced by adding the inducer DOX. The iPSC colonies were quantitated by immunohistochemical staining of the pluripotent marker NANOG (red). The shRNA knockdown of *Pel*1 was tracked by the copGFP maker in the lentiviral vector. (B) Knockdown of *Pel*1 by shRNA in fibroblasts. After lentiviral shRNA transfection, fibroblasts were selected by puromycin and collected for Q-PCR. shCT: random shRNA control; shPel1: *Pel*1 shRNA. For comparison, the abundance of *Pel*1 in vector controls was set as 1. (C) Reprogramming efficiency. The iPSC colonies were quantitated by immunohistochemical staining of the pluripotent marker NANOG. shPel1-1 and shPel1-2: shRNAs that target the *Pel*1 lncRNA; shCT: random control shRNA; Vector: the lentiviral vector control. (D) Expression of stem cell core factors. Cells were collected and used for PCR quantitation for *Pel*1 and stem cell core factors. All the data are presented as mean \pm SD of three independent experiments. ***, $P < 0.001$; **, $P < 0.01$; *, $P < 0.05$; NS, not significant as compared with the Vector control group.

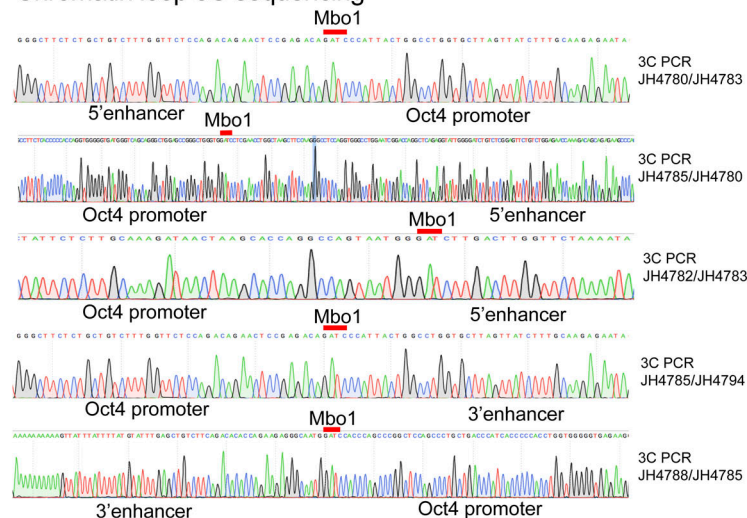
A *Pelnl* binds to *Oct4*



B *Pelnl* affects chromatin loop



C Chromatin loop 3C sequencing



suggesting the involvement of a base-pairing pathway in the *Pelnl*-*Oct4* interaction.

Pelnl induces *Oct4* DNA methylation by recruiting DNMT3A

The *Oct4* promoter is epigenetically regulated by DNA methylation of CpG islands. We compared the methylation status of two CpG islands in the *Oct4* promoter. Genomic DNAs were isolated from the untreated iPSC control, vector control, and

Figure 5. *Pelnl* binds to *Oct4* and dismantles intra-chromosomal looping. (A) Binding of *Pelnl* in the *Oct4* locus by Q-PCR. In the RAT-seq assay, chromatin *Pelnl* lncRNA was reverse transcribed using *Pelnl*-specific antisense primers (*Pelnl*) and biotin-dCTP. The random oligonucleotides (CtI) were used as the RAT control. Q-PCR was used to map the interaction using primers located in the *Oct4* locus. Enh: enhancers; p*Oct4*: *Oct4* promoter; A-N: location of PCR primers used to detect the interaction between *Pelnl* and *Oct4*. 5'-CtI: the 5'-Control site; 3'-CtI-3'-Control; 5'-Enh: 5'-enhancer; 3'-Enh: 3'-Enhancer; E1-E5: *Oct4* exons 1-5. Note the binding of *Pelnl* in the *Oct4* promoter and 3'-enhancer. Data are presented as mean \pm SD of three independent experiments. (B) *Pelnl* is essential for maintaining normal intrachromosomal looping. Top panel: Location of 3C primers used to detect the interaction between the *Oct4* promoter and enhancer. Enh: enhancers; p*Oct4*: *Oct4* promoter; E1-E5: *Oct4* exons; Arrows: intrachromosomal interactions. Blue arrows with red crosses represent the loops that disappeared after *Pelnl* overexpression in E14 cells. Bottom panel: Binding frequency of the *Oct4* promoter and enhancers in E14 cells. After 3C, the interaction frequency was quantitated by Q-PCR. *Pelnl*: The *Pelnl*-expressing cells; Vector: control vector-expressing cells. Data are presented as mean \pm SD of three independent experiments. (C) Sequencing confirmation of the intrachromosomal 3C products. Red line on the top of the sequence: the 3C ligation product at the *Mbo*I site, which is flanked by the *Oct4* promoter and enhancer sequences.

Pelnl-overexpressing E14 cells. After sodium bisulfite treatment using an EZ DNA Methylation-Gold Kit, genomic DNAs in the *Oct4* promoter were amplified and digested with restriction enzymes to separate the methylated and unmethylated CpGs. Overexpression of *Pelnl* induced DNA methylation at CpG1 and CpG2 sites in the *Oct4* promoter, in parallel with the down-regulation of the stem cell marker gene (Fig. 6 A). These data suggest that the lentivirus-induced overexpression of *Pelnl*

bound to the *Oct4* promoter and silenced it by altering the promoter epigenotype. In fibroblasts, however, silencing of *Pelnl* only induced a slight change in CpG methylation at the *Oct4* promoter (Fig. S3 D), suggesting that other factors, in addition to *Pelnl*, may be also required for the maintenance of DNA methylation in fibroblasts.

The status of DNA methylation in the *Oct4* promoter is controlled by the three active DNA methyltransferases, DNMT1, DNMT3A and DNMT3B. We found that Dnmt3a was significantly upregulated in *Pelnl*-overexpressing E14 cells (Fig. S4 A), although it did not result in a significant change in EB differentiation (Fig. S4 B). We then used RNA immunoprecipitation (RIP) to determine if the binding of *Pelnl* to the *Oct4* promoter might recruit this DNA methyltransferase, thereby accounting for the induced DNA demethylation. The chromatin complex in *Pelnl*-overexpressing E14 cells was immunoprecipitated with an anti-DNMT3A antibody. After RNA purification and reverse transfection, we quantitated the presence of *Pelnl* lncRNA in the immunoprecipitated products using primers that cover the different locations of *Pelnl* lncRNA and showed that DNMT3A interacted primarily with the 3'-fragment of *Pelnl* (Fig. 6 B). However, expression of *Pelnl* did not recruit DNMT3B and DNMT1 to the *Oct4* promoter (Fig. S4 C).

We confirmed this interaction by incubating DNMT3A recombinant protein with different biotin-labeled *Pelnl* lncRNA fragments. After streptavidin bead pulldown, Western blotting was used to detect the interaction with DNMT3A. In agreement with the above RIP assay, we found that *Pelnl* primarily utilized its 3'-terminal 100 bp fragment to recruit DNMT3A (Fig. 6 C).

We also used chromatin immunoprecipitation to validate the binding of DNMT3A at the *Oct4* locus. *Pelnl*-overexpressing E14 cells and control cells were immunoprecipitated with a DNMT3A antibody. The immunoprecipitated chromatin DNAs were purified and examined for binding of DNMT3A. No significant enrichment signals were detected in the untreated and vector control cells. However, we detected binding of DNMT3A at the *Oct4* promoter in a pattern similar to the binding of *Pelnl* (Fig. 6 D). Expression of the *Pelnl* 3'-terminal-deleted mutant failed to alter CpG methylation (Fig. S5 A), recruit DNMT3A (Fig. S5 B), or downregulate the *Oct4* in E14 cells (Fig. 6 E). These data suggest that *Pelnl* plays a dual role in the epigenetic regulation of *Oct4*, upregulating DNMT3A at the transcriptional level and recruiting DNMT3A enzyme to the *Oct4* promoter.

Discussion

As a new class of epigenetic regulators, lncRNAs play a critical role in the maintenance of stem cell pluripotency. Depending on the intracellular localization, an lncRNA may regulate pluripotency maintenance using different mechanism (Chen et al., 2020). Nuclear lncRNAs usually regulate pluripotency-associated marker genes by interacting with chromatin modification factors, RNA binding proteins, or transcription factors. In contrast, cytoplasmic lncRNAs are functionally different from nuclear lncRNAs and mainly act as posttranscriptional regulators by modulating mRNA degradation and protein translation.

However, the molecular components of the epigenetic regulatory circuitry in pluripotency exit have not been fully characterized. Exit from pluripotency and stem cell differentiation require precise regulation of this pluripotency network. In this study, we profiled pluripotency exit-associated lncRNAs by combining three sequencing datasets: the lncRNA interaction network in the stem cell core factor gene *Oct4*, the differential transcriptome during pluripotent reprogramming, and the lncRNA genome-wide gene target interactome. Using this approach, we identified *Pelnl* as a critical lncRNA that determines the exit of E14 cells from pluripotency. *Pelnl* is actively transcribed in fibroblasts and tissues and becomes silenced in pluripotent reprogramming. Overexpression of this lncRNA induced the exit of E14 cells from pluripotency. In contrast, knockdown of *Pelnl* enhances reprogramming efficiency. *Pelnl* triggers exit from pluripotency through the dual mechanism of upregulating Dnmt3a and recruiting it to the *Oct4* promoter, thereby altering the promoter epigenotype and abrogating pluripotency-specific intrachromosomal architecture. This study provides the first evidence that a lncRNA can epigenetically control the exit from stem cell pluripotency by *trans* targeting the *Oct4* promoter (Fig. 6 E).

In stem cells, the transcriptional regulatory circuitry that controls the ground pluripotent state is maintained by coordinated expression of the core transcription factors *Oct4*, *Sox2*, and *Nanog*. The exit from pluripotency requires the dismantling of this gene expression circuitry. As a critical stem cell core transcription factor, *Oct4* is actively transcribed in pluripotent stem cells, but is transcriptionally silenced in somatic cells. We hypothesized that a pluripotency exit-associated lncRNA would have the ability to negatively regulate the *Oct4* promoter. We demonstrate that *Pelnl* interacts with the *Oct4* promoter, recruiting the DNA methyltransferase DNMT3A, which induces de novo DNA methylation and thereby inhibits promoter activity. Decreased expression of *Oct4* initiates the exit of stem cells from pluripotency.

Currently, it is not clear how this lncRNA recognizes its target genes. Using LongTarget lncRNA-DNA interaction prediction software (He et al., 2015), we found that nearly all the predicted *Pelnl*-*Oct4* binding sites were aggregated in a short fragment of 5'-*Pelnl*. Deletion of this short fragment caused the loss of this *Pelnl* function. Together, these data suggest that this lncRNA may use a Hoogsteen base-pairing mechanism to bind to the *Oct4* promoter. However, other chromatin factors, like CTCF and Cohesin, might be also involved in this lncRNA-chromatin DNA interaction.

Exit from pluripotency and priming for differentiation into somatic lineages is associated with genome-wide de novo DNA methylation. This is a dynamic regulatory system, which is critical for coordinating pluripotent exit with early lineage specification. Exit from the ESC state requires dissolution of the core pluripotency transcription-factor circuit, but how the differentiation machinery breaks down this network is unclear. In response to differentiation cues, the cell can activate distinct lineage-specific gene networks while turning off or rewiring pluripotency networks. The molecular components that coordinate this pluripotent exit are poorly understood.

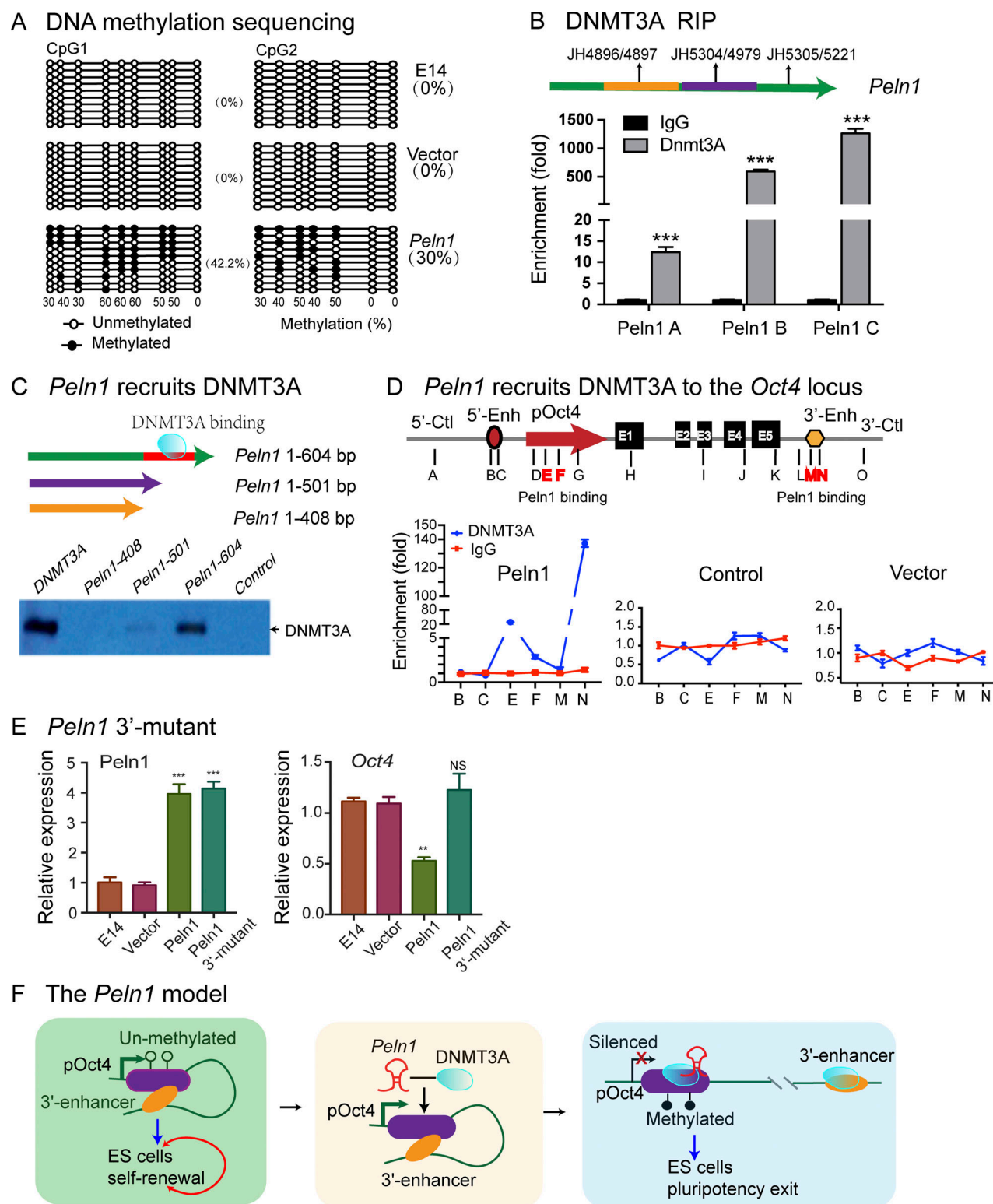


Figure 6. *Peln1* induces DNA methylation in Oct4 by recruiting DNMT3A. (A) *Peln1* induces DNA methylation in the *Oct4* promoter. DNA methylation was quantitated with a EZ DNA Methylation-Gold Kit and PCR products were sequenced to distinguish methylated and unmethylated DNAs. CpG1, CpG2: CpG islands in the *Oct4* promoter. E14: E14 control; vector: lentiviral vector control; *Peln1*: *Peln1*-overexpressing E14 cells; empty circles: unmethylated CpGs; solid circles: methylated CpGs. (B) Quantitation of the *Peln1*-DNMT3A interaction by RIP. The anti-DNMT3A antibody pulldown RNAs were reverse transcribed, and Q-PCR was used to compare the interaction frequency of the *Peln1* fragments (A, B, C). The anti-IgG antibody was used as an immunoprecipitation control. Data are presented as mean \pm SD of three independent experiments. ***, $P < 0.001$ as compared with the IgG control group. (C) The *Peln1*-DNMT3A binding assay: Three *Peln1* lncRNA fragments (1-408 bp, 1-501 bp, and full length 604 bp) were synthesized using a HiScribeTM T7 Quick High Yield RNA Synthesis Kit (NEB) with biotin-CTP. The *Peln1* lncRNA fragments were purified by streptavidin beads and were incubated with DNMT3A protein in vitro. After bead washing, the

Pelnl-intreated DNMT3A proteins were eluted for Western blot detection. Note the strong binding of DNMT3A at the 3'-end of *Pelnl* lncRNA. **(D)** *Pelnl* recruits DNMT3A to the *Oct4* locus. The *Pelnl*-DNMT3A interaction was assayed by immunoprecipitation. Data are presented as mean \pm SD of three independent experiments. Note the increased binding of DNMT3A to the *Oct4* locus in the *Pelnl*-overexpressed cells. **(E)** DNMT3A-binding element-deleted *Pelnl* mutant lacks a regulatory role in pluripotency. E14 cells were transfected with the WT *Pelnl* and the mutant *Pelnl* that lacks the DNMT3A-binding element. The empty lentiviral vector was used as the control. The role of *Pelnl* was examined by quantitating the expression of pluripotent marker *Oct4*. Data are presented as mean \pm SD of three independent experiments. ***, $P < 0.001$; **, $P < 0.01$; *, $P < 0.05$; NS, not significant as compared with the Vector control group. **(F)** Model of *Pelnl* in exit from pluripotency. In pluripotent stem cells, *Oct4* is unmethylated. An intrachromosomal loop juxtaposes the distal enhancer in close proximity with the promoter. The expression of this endogenous core stem cell factor is an essential step to maintain pluripotency and self-renewal. *Pelnl* upregulates DNMT3A and recruits the DNA methyltransferase to the *Oct4* promoter, thereby altering the promoter epigenotype. *Pelnl* also induces the loss of the pluripotency-specific intrachromosomal architecture.

The maintenance of the pluripotent identity also requires a precisely regulated 3D chromatin interaction network composed of intra- and interchromosomal loops and bridges (Denholtz et al., 2013; Ji et al., 2016; Sexton and Cavalli, 2013). By comparing the “non-iPSCs” that failed to complete pluripotent reprogramming, we found that the virally expressed OSKM factors bound to their target genes, but could not activate them to achieve pluripotency due to the lack of a promoter-enhancer intrachromosomal loop architecture (Zhang et al., 2013). Formation of this intrachromosomal loop is a critical epigenetic barrier that must be overcome for induction of pluripotency, as it juxtaposes the distal enhancer in close proximity with the promoter for activation. Notably, the CRISPR Cas9-enforced formation of functional intrachromosomal looping alters the epigenotypes in the *Oct4* promoter, thereby activating the pluripotent gene (Morgan et al., 2017). Using the same dCas9-ABA-inducible system, Wang et al. (2021) recently showed that this artificial chromatin linking enhanced reprogramming efficiency. However, it is not clear how DNA methylation is involved with the pluripotency chromatin loop in *Oct4*. *Pelnl* actively participates in the regulation of this pluripotency-specific 3D interaction, acting as a regulatory chromatin factor. After binding to the *Oct4* promoter, *Pelnl* disrupts this intrachromosomal interaction, leading to exit from pluripotency. These results suggest a master regulatory role of *Pelnl* in maintaining pluripotency of stem cells.

In summary, the ability of a stem cell to self-renew or to exit from pluripotency is controlled by a tightly regulatory circuitry consisting of transcriptional factors, chromatin architecture, and epigenetic modifications. In this study, we have provided the first evidence that lncRNA *Pelnl* acts as a new epigenetic player in this regulatory circuitry. By binding to numerous pathway genes, particularly *Oct4*, *Pelnl* plays a “fine-tuning” role in shutting down the regulatory network conferring pluripotency and ultimately induces dissolution of the pluripotent state in E14 cells. The findings presented here may have broad implications for other chromatin-associated lncRNAs in the epigenetic regulation of stem cell pluripotency. Most notably, by quantitating three lineage markers in *Pelnl*-expressing E14 cells, we noticed that *Pelnl* induced cell differentiation in favor of the endoderm lineage by expressing higher endoderm markers, including *PDX1* and *NKX6-1* (Fig. 3 C). This useful finding may suggest its application in regenerative medicine. Future studies are encouraged to determine if *Pelnl* can promote the formation of endoderm-related organs, such as pancreatic β cells in the treatment of diabetes.

Materials and methods

Cell lines and cell culture

Mouse fibroblasts and 293T cells were cultured in DMEM containing 10% (vol/vol) FBS (Sigma-Aldrich), 1% (vol/vol) of penicillin-streptomycin (Sigma-Aldrich) at 37°C in a 5% CO₂ air atmosphere. E14 and IPS cells were cultured in knockout DMEM containing 15% (vol/vol) KnockOut SR (Gibco), 1% (vol/vol) of penicillin-streptomycin (Sigma-Aldrich), 200 μ M β -mercaptoethanol, 1,000 U/ml lif (Millipore), 1XMEM-NEAA at 37°C in a 5% CO₂ air atmosphere.

E14 mouse ESCs in the naive status were purchased from ATCC. Pluripotent cells were induced into the primed status by culturing E14 cells under culture conditions including FGF2 (12 μ g/ml) and Activin A (20 μ g/ml) in the absence of LIF (Tosolini and Jouneau, 2016).

CRIST-seq to map the *Oct4*-interacting lncRNAs

To profile the *Oct4* promoter-interacting lncRNAs, we constructed the Cas9-*Oct4* gRNA vector by cloning two *Oct4* promoter gRNAs into the lenti Cas9 gRNA vector that contains the catalytically inactive Cas9 (dCas9). *Oct4*-gRNA1: 5'-GAACATTCAATGGATGTTTT-3' and *Oct4*-gRNA2: 5'-GTGTGAGGGGATTGGGGCTC-3' (Table S1). For CRIST-seq control, we performed a CRIST assay using a random gRNA (gCT5'-GAAGTGGGATGATCCTCTGA-3'; Table S1). The dCas9-gRNA lentiviruses were packaged in 293T cells.

Fibroblasts were transfected with dCas9-gRNAs lentiviruses produced by 293T cells. After transfection, cells were selected with puromycin and collected for immunoprecipitation. Cells were cross-linked with 2% formaldehyde and lysed with cell lysis buffer (10 mM Tris [pH 8.0], 10 mM NaCl, 0.2% NP-40, and 1 \times protease inhibitors). After centrifugation, DNA was reverse transcribed at 37°C for 30 min in a 20- μ l reaction (1 μ l random hexamer, 1 μ l 10 mM dNTP, 1 μ l 0.4 mM biotin-dCTP, 1 μ l RT enzyme, 0.5 μ l RNase inhibitors, 1 μ l 0.1 M DTT, 4 μ l 5 \times cDNA synthesis buffer, 1 μ l Maxima Reverse Transcriptase, and RNase-free water to 20 μ l). The reaction was stopped by adding 4 μ l 0.5 M EDTA. The chromatin complex was subjected to sonication for 180 s (10 s on and 10 s off) on ice with a Branson sonicator with a 2-mm microtip at 40% output control and 90% duty cycle settings. The biotin-labeled cDNA/Cas9 complex was immunoprecipitated with anti-FLAG antibodies (#MA1-91878; Thermo Fisher Scientific, IL, or #F7425; Sigma-Aldrich). The DNAs were released after cross-linking reversal and proteinase K treatment. The biotin-labeled cDNAs were further purified from genomic DNAs with M-280 streptavidin beads (Invitrogen). The

Oct4 promoter-interacting cDNAs were subjected to Illumina sequencing (Zhang et al., 2019). The lncRNA-*Oct4* interaction was quantitated by Q-PCR using target gene primers (Table S1).

RNA-seq

For RNA-seq, total RNA was isolated from fibroblasts and iPSCs (Zhai et al., 2015; Zhang et al., 2013) using TRIzol (Invitrogen). RNA-seq was performed by Shanghai Biotechnology using a HiSeq4000 (Illumina). Differentially expressed RNAs in fibroblasts and iPSCs were defined using a cutoff threshold of more than twofold, $P < 0.05$ (Du et al., 2018).

Identification of *Pelnl* target genes by RAT-seq

A RAT assay (Du et al., 2018) was modified to identify the interacting target genes of *Pelnl*. Specifically, cells were cross-linked with 2% formaldehyde and lysed with cell lysis buffer (10 mM Tris [pH 8.0], 10 mM NaCl, 0.2% NP-40, and 1× protease inhibitors). Gene strand-specific reverse transcription was performed in the presence of biotin-dCTP. After 30 min of reverse transcription of *Pelnl* lncRNA with Maxima Reverse Transcriptase (Thermo Fisher Scientific) at 62°C, the reaction was stopped by adding 4 μl 0.5 M EDTA. The chromatin complex was then subjected to sonication for 180 s (10 s on and 10 s off) on ice with a Branson sonicator with a 2-mm microtip at 40% output control and 90% duty cycle settings. The biotinylated-lncRNA-cDNA/chromatin DNA complex was pulled down with biotin-streptavidin magic beads (Invitrogen). After reversing the cross-links and treatment with 10 mg/ml proteinase K at 65°C for 2 h, the genomic DNA that interacted with the lncRNA was extracted, digested by MboI, and ligated with the NEBNext adaptors (NEBNext ChIP-Seq Library Prep Master Mix Set for Illumina) to construct the library. The library DNAs were subjected to Illumina sequencing (Shanghai Biotechnology). We performed a RAT assay by replacing *Pelnl* complementary primers with random primers for RAT-seq control, and constructed a control library for sequencing.

After RAT sequencing, the low-quality reads were filtered. Clean reads were mapped to the mouse genome (genome version: mm10). By comparing the RAT-seq peaks with input samples, enriched regions of the genome were identified using MACS2 (version: 2.1.1). The upstream 2 kb of the transcription start sites and the downstream 5 kb of the transcription termination region were defined as the gene regions. The significant GO terms of biological processes with a P value < 0.05 were selected. To reduce the background, the RAT-seq data were further normalized over the peaks of the control RAT-seq data that were generated by using random oligonucleotide primers in the RAT assay.

Reprogramming-associated RNA candidates were identified by RNA-seq using a cutoff threshold of more than twofold, $P < 0.05$. *Pelnl* target genes were identified using a RAT. The top 40 genes, sorted by expression differences from high to low in iPSC, were selected for further study.

5'- and 3'-RACE of *Pelnl* lncRNA

The full-length *Pelnl* lncRNA was characterized by cDNA 5'- and 3'-RACE (Sun et al., 2014). For 3'-end RACE, we used the 3'-RACE

system for rapid amplification of cDNA ends (1446137; Invitrogen). For 5'-RACE, the Fib RNAs were reverse transcribed using Maxima Reverse Transcriptase with random hexamer oligonucleotides for 30 min. The poly G primer J526: 5'-CCAGATTCAGGACTGTCGACATCGAATTCGGGG-3' was added to the mixture and the reaction was allowed to continue for another 30 min. After 10-fold dilution, the first RACE PCR was performed using a 3'-RACE primer J527: 5'-GATTGAGGACTGTCGACATCGA-3' and a 5'-*Pelnl*-specific primer JH4980: 5'-CTCCTATTATGTACTACAGAGTTC-3'. DNAs were diluted 500-fold and were used for the second nested PCR using a 3'-RACE primer J527: 5'-GATTGAGGACTGTCGACATCGA-3' and 5'-*Pelnl*-specific primer JH5149: 5'-AGCCCTACTGGTACTATGGTA-3'. The RACE PCR bands were cut out and cloned into a pjet vector for sequencing.

Cytoplasmic and nuclear fractionation assay

Cells were spun down in Falcon tubes for 5 min at 3,000 rpm in a Beckman tabletop centrifuge, washed once with PBS, and spun again for 5 min at 3,000 rpm. After completely aspirating the PBS, 800 μl of hypotonic buffer (10 mM Hepes, pH 7.9, 1.5 mM MgCl₂, and 10 mM KCl) was added to each sample, the pellet was gently resuspended, transferred to a microfuge tube, and placed in ice for 2 min. Through the remaining steps of the protocol, samples were kept on ice and spun at 4°C. 10% Nonidet P-40 was added to a final concentration of 0.4% (35 μl). Samples were inverted a few times and spun at 3,000 rpm for 7 min. Supernatants (450 μl; cytoplasmic fractions) were collected for processing, and the remaining supernatants were discarded. Then, the pellet (nuclear fraction) was gently resuspended in 500 μl of hypotonic buffer and spun at 3,000 rpm for 2 min. This washing step was repeated three to four times. After removing the buffer following the last spin, the samples were briefly spun once again to remove the remaining supernatant from the cells. Both the cytoplasmic and nuclear fractions were processed following the RNA extraction protocol as recommended by the manufacturer.

Overexpression and knockdown of *Pelnl* lncRNA

The full length of *Pelnl* lncRNA was amplified by PCR and ligated into the EcoRV/EcoRI site in 1× Spanch2 vector. *Pelnl* lncRNA was knocked down by two separate shRNA lentiviral vectors (shPelnl-1 and shPelnl-2). The shRNA vectors were constructed by cloning four shRNAs into two separate pGreenPuro vectors (#SI505A-1, SBI), each containing two shRNAs. For cloning, shRNAs were linked to the H1 and U6 promoters using PCR and were ligated into the EcoRI/BamHI site in pGreenPuro vector (SBI). The copGFP reporter in the vector was used to track the lentivirus transfection in E14 cells.

Cell reprogramming

MEFs were derived from transgenic mice that carried DOX-inducible OSKM genes. The four reprogramming factors, OSKM, were expressed from the collagen type 1 gene locus upon induction with DOX (Carey et al., 2010). MEFs were cultured in MEF medium (DMEM supplemented with 10% FBS, 1% P/S, 1% GlutaMAX, and 1% NEAA), according to standard methods at 5% CO₂ and 37°C (Kleger et al., 2012). The *Pelnl* shRNA1-1 and shRNA1-2 and control shRNA lentiviruses were packaged in

293T cells using lipofectamine 3000 (Invitrogen). The virus-containing supernatants were collected and concentrated with Centrifugal Filter Units (Amicon Ultra-15; Millipore). MEFs in 6-well plates were infected with lentiviruses. 3 d after infection, the cells were digested and transferred to a p12 plate at 15,000–20,000 cells/well. On the following morning, the medium was changed into serum-KSR iPS medium (10% FBS, 10% KSR, 1% P/S, 1% GlutaMAX, 1% NEAA, 1% sodium pyruvate, 0.1% β -mercaptoethanol, 1,000 U/ml LIF) containing 2 μ g/DOX. iPSC medium was changed every other day for the first 3–5 d before cells become confluent and every day thereafter. On day 12–15, immunostaining was performed, and the *Nanog* positive iPSC colonies were counted.

Mapping the DNMT3A-lncRNA interactome by RIP

Fibroblasts were collected for immunoprecipitation. In order to map the DNMT3A-lncRNA interactome, the biotinylated lncRNA-cDNA/Dnmt3a complex was immunoprecipitated with anti-DNMT3A antibodies (ab88470; Abcam). The biotinylated lncRNA-cDNAs were further purified from genomic DNAs using M-280 streptavidin beads (Invitrogen; Zhang et al., 2014b). After purification, the DNMT3A-interacting lncRNA-cDNAs were quantitated by PCR using target gene primers.

Luciferase reporter assay

The 2 kb of *Oct4* promoter was amplified and then inserted into the pGL3vector (Promega) to create a luciferase reporter construct, which was named pGL3-OCT4. E14 cells (1×10^6) were cotransfected with 500 ng of pGL3-OCT4, 2 μ g of *Pelnl*-overexpressing plasmid, and 100 ng of a Renilla luciferase expression construct pRL-TK (Promega) using Lipofectamine 3000. Luciferase activity was then measured with the dual luciferase assay system (Promega) after 48 h of transfection. Renilla luciferase activity was used as the internal control for normalization.

Immunohistochemical staining of stem cell markers

Immunofluorescence staining was used to examine stem cell markers in iPSC colonies (Chen et al., 2012). Briefly, cells were fixed by 4% paraformaldehyde/PBS for 10–15 min and rinsed with PBS, then permeabilized and blocked with 0.1% Triton X-100/PBS containing 3% BSA for 30 min. After incubation with primary antibodies for 1 h at room temperature or overnight at 4°C, the samples were washed three times with PBS, and then incubated with secondary antibody for 1 h. The following antibodies were used in the immunostaining: rabbit anti-NANOG (sc-33759, 1:100 dilution; Santa Cruz Biotechnology) and rabbit anti-OCT4 (AB3029, 1:100 dilution; Millipore). The cell samples were subsequently incubated with Cy3- or Alexa Fluor 488-labeled secondary antibodies for 1 h. After washing three times with PBS, samples were counterstained with Hoechst 33258 (Invitrogen). Alternatively, the pluripotency of stem cells was examined using a Fluorescent Mouse ES/iPS Cell Characterization kit (Cat. no. SCR077; Millipore) following the protocol provided by the manufacturer. Fluorescence images were acquired with a Zeiss AxioCam Camera.

Embryoid body differentiation

For embryoid body (EB) formation, iPSCs or E14 cells were trypsinized by collagenase IV (Invitrogen), and cell clumps were transferred to 60-mm dishes in ES medium without LIF. After being maintained in floating culture for 3 d, the EB was seeded in 0.1% gelatin-coated 6-well plates in DMEM/F12 containing 20% FBS to allow for spontaneous differentiation. Cells were collected at different time points and used for gene expression analysis using Q-PCR.

DNA methylation analysis

Genomic DNAs were extracted from E14 cells, E14+control vector cells, and E14+*Pelnl*-overexpressing cells and treated with a EZ DNA Methylation-Gold Kit (Cat. no. D5005). Methylation PCR was performed, and PCR DNAs were cloned into pJet vector for sequencing (Zhang et al., 2014a). After treatment with the Methylation Kit, unmethylated cytosines were converted to uracils, which can be distinguished from the methylated cytosines by sequencing (Ma et al., 2014; Zhao et al., 2016).

Quantitation of intrachromosomal looping by 3C

The chromosome conformation capture (3C) assay was performed to determine intrachromosomal interactions (Du et al., 2021). Briefly, fibroblasts and iPSCs were cross-linked with 2% formaldehyde and lysed with Hi-C Lysis buffer (10 mM Tris-HCL, pH 8.0, 10 mM NaCl, 0.2% NP-40, 1 \times protease inhibitors). An aliquot of nuclei (2×10^6) was digested with 100 U *MboI* at 37°C 2 h. Chromatin DNA was diluted with NEB ligation buffer and ligated with 2,000 U of T4 DNA ligase. After reversing the cross-links, DNA was purified and used for PCR amplification using primers that are derived from different regions of the *Oct4* locus. The 3C PCR products were cloned and sequenced to validate the intrachromosomal interaction by determining the presence of the *MboI* ligation site (Li et al., 2008).

RT-PCR

Total RNA was extracted with TRIzol reagent (Sigma-Aldrich) from cells and stored at -80°C . RT-PCR was performed with a Bio-Rad Thermol Cycler. The target amplification was performed by PCR of 1 cycle at 95°C for 5 min, 33 cycles at 95°C for 20 s, 62°C for 15 s and 72°C for 15 s, and 1 cycle at 72°C for 10 min. Quantitative RT-PCR was performed using SYBR GREEN PCR Master (Applied Biosystems). The threshold cycle (Ct) values of target genes were assessed by Q-PCR in triplicate using a sequence detector (ABI Prism 7900HT; Applied Biosystems) and were normalized over the Ct of the β -actin control.

DNMT3A-Oct4 interaction by ChIP

The DNMT3A-Oct4 interaction was measured by chromatin immunoprecipitation (ChIP; Schulz and Haussler, 2014). One million E14 cells, E14 cells with 1xSpanch2 vector, and E14 cells with *Pelnl* overexpression were harvested. The DNA/Dnmt3a complex was immunoprecipitated with anti-Dnmt3a antibodies (ab88470; Abcam). After purification, the Dnmt3a-interacting DNAs were quantitated by PCR using target gene primers (Table S1).

Pelnl-DNMT3A binding assay

Pelnl lncRNA was synthesized using a HiScribe™ T7 Quick High Yield RNA Synthesis Kit (NEB) with biotin-CTP. The biotinylated *Pelnl* lncRNA was purified for the following RNA-protein binding assay. Briefly, The EP tubes containing prepared streptavidin agarose are refilled with 500 µl of streptavidin washing buffer (20 mM Tris-HCl, pH 7.5, 100 mM KCl, 2 mM EDTA, 0.5 mM DTT, and 0.5 mM PMSF) and gently pipetted 4–5 times with an end-cut blue tip. 1 µl (100 pmol) of biotin-labeled RNA is applied to the EP tubes except for the EP tubes that served as negative controls. EP tubes are incubated at 4°C for 1–4 h under 100 RPM rotation in a rotator. After washing twice with 500 µl of the RNA-streptavidin interaction buffer (20 mM Tris-HCl, pH 7.5, 300 mM KCl, 0.2 mM EDTA, 0.5 mM DTT, and 0.5 mM PMSF), 1 µg of Dnmt3a protein is applied to each of above EP tubes. The reaction was maintained at 4°C overnight (about 12 h) under 100 RPM rotation. On the following day, the preparation is washed twice with RNA-streptavidin interaction buffer. 16 µl of 1× protein loading dye is applied to each EP tube obtained from above procedure. The EP tubes are heated at 80°C for 5 min and then the *Pelnl*-interacting DNMT3a was detected by Western blotting.

Quantitation of CRIST and RAT signals by Q-PCR

In both CRIST and RAT assays, quantitative RT-PCR was used to compare the enrichment signals between treatment groups. Q-PCR was performed using SYBR GREEN PCR Master (Applied Biosystems) in triplicate using a sequence detector (ABI Prism 7900HT; Applied Biosystems; Bao et al., 2015; Li et al., 2014). The enrichment signals were calculated using threshold cycle (Ct) values standardized over the input, applying the $2^{-(\Delta Ct)}$ method.

Statistical analysis

All the experiments were repeated three times and were analyzed using SPSS software (version 16.0, Inc.). The Kolmogorov-Smirnov test was used to test the data normality. One-way ANOVA with Bonferroni's multiple comparisons test was used to compare statistical differences for selected variables among treatment groups. Differences were considered significant for P values < 0.05 (*, P < 0.05; **, P < 0.01; ***, P < 0.001).

Online supplemental material

Table S1 shows the oligonucleotide primers used for PCR and RAT assays. Fig. S1 maps the pluripotency exit-associated lncRNAs by CRIST-seq. Fig. S2 characterizes the *Pelnl* promoter and *Pelnl* expression in tissues. Fig. S3 examines the role of *Pelnl* and its mutant in the *Oct4* promoter methylation and colony formation. Fig. S4 shows the data of DNA methyltransferases expression and ChIP-*Oct4* assay. Fig. S5 shows that the *Pelnl* 3'-mutant failed to induce DNA methylation in the *Oct4* promoter.

Data availability

As previously reported (Du et al., 2018), the CRIST-seq, RAT-seq, and RNA-seq data generated in this study have been deposited in NIH GEO databases under accession nos. GSE137769, GSE107945, GSE101765, and GSE116605, respectively.

Acknowledgments

This work was supported by the National Key R&D Program of China (2018YFA0106902, 2020YFA0707704), the Innovative Program of National Natural Science Foundation of China (82050003), the National Natural Science Foundation of China (31871297, 81874052, 81900701, 81900327, 82001670, 82101675, 32000431), the Fund of Jilin Provincial Science and Technology Department (20210101311JC, 20190303146SF, 20200602032ZP, 20200201390JC), the Provincial Science Fund of Jilin Province Development and Reform Commission (2021C10 and 2020C038-4), the Natural Science Fund of Jilin Provincial Finance Department (JLSWSRCZX2020-023, JLSWSRCZX2020-100), the Youth Fund of Jilin Provincial Health Commission (2016Q035), the Fund of Changchun City Science and Technology Bureau (21ZGY28), China Guanghua Fund and the Youth Fund of First Hospital of Jilin University (2020-CXM-01, JDYYGH2019004, JDYY 102019002, JDYY 102019034), California Institute of Regenerative Medicine (CIRM) grant (RT2-01942), and the Department of Veterans Affairs (BX002905).

The authors declare no competing financial interests.

Author contributions: Y. Wang and L. Jia designed and performed assays for the study. C. Wang and X. Wen performed cell reprogramming and cell culture studies. Z. Du, S. Zhang, and L. Zhou performed the CRIST-seq assay and RNA-seq. H. Li, H. Chen, Y. Nie, D. Li, and S. Liu conducted some Q-PCR and RT-PCR studies. D.S. Figueroa and F. Ay contributed to bioinformatics analyses of RNA-seq, CRIST-seq, and RAT-seq data. J.-F. Hu, A.R. Hoffman, W. Xu, S. Zhang, W. Li, J. Cui, and H. Guo contributed to the study design and supported the study. J.-F. Hu wrote the manuscript and A.R. Hoffman edited the manuscript. The authors read and approved the final manuscript.

Submitted: 24 September 2020

Revised: 1 December 2021

Accepted: 19 January 2022

References

- Bao, X., H. Wu, X. Zhu, X. Guo, A.P. Hutchins, Z. Luo, H. Song, Y. Chen, K. Lai, M. Yin, et al. 2015. The p53-induced lncRNA-p21 derails somatic cell reprogramming by sustaining H3K9me3 and CpG methylation at pluripotency gene promoters. *Cell Res.* 25:80–92. <https://doi.org/10.1038/cr.2014.165>
- Betschinger, J., J. Nichols, S. Dietmann, P.D. Corrin, P.J. Paddison, and A. Smith. 2013. Exit from pluripotency is gated by intracellular redistribution of the bHLH transcription factor Tfe3. *Cell.* 153:335–347. <https://doi.org/10.1016/j.cell.2013.03.012>
- Cao, H., D. Xu, Y. Cai, X. Han, L. Tang, F. Gao, Y. Qi, D. Cai, H. Wang, M. Ri, et al. 2021. Very long intergenic non-coding (vlinc) RNAs directly regulate multiple genes in cis and trans. *BMC Biol.* 19:108. <https://doi.org/10.1186/s12915-021-01044-x>
- Carey, B.W., S. Markoulaki, C. Beard, J. Hanna, and R. Jaenisch. 2010. Single-gene transgenic mouse strains for reprogramming adult somatic cells. *Nat. Methods.* 7:56–59. <https://doi.org/10.1038/nmeth.1410>
- Chen, J., Y. Wang, C. Wang, J.F. Hu, and W. Li. 2020. LncRNA functions as a new emerging epigenetic factor in determining the fate of stem cells. *Front. Genet.* 11:277. <https://doi.org/10.3389/fgene.2020.00277>
- Chen, M., H. Zhang, J. Wu, L. Xu, D. Xu, J. Sun, Y. He, X. Zhou, Z. Wang, L. Wu, et al. 2012. Promotion of the induction of cell pluripotency through metabolic remodeling by thyroid hormone triiodothyronine-activated PI3K/AKT signal pathway. *Biomaterials.* 33:5514–5523. <https://doi.org/10.1016/j.biomaterials.2012.04.001>

- Chen, N., X. Yan, G. Zhao, Z. Lv, H. Yin, S. Zhang, W. Song, X. Li, L. Li, Z. Du, et al. 2018. A novel FLI1 exonic circular RNA promotes metastasis in breast cancer by coordinately regulating TET1 and DNMT1. *Genome Biol.* 19:218. <https://doi.org/10.1186/s13059-018-1594-y>
- Chen, Y., H.N. Chen, K. Wang, L. Zhang, Z. Huang, J. Liu, Z. Zhang, M. Luo, Y. Lei, Y. Peng, et al. 2019. Ketoconazole exacerbates mitophagy to induce apoptosis by downregulating cyclooxygenase-2 in hepatocellular carcinoma. *J. Hepatol.* 70:66–77. <https://doi.org/10.1016/j.jhep.2018.09.022>
- Dekker, J., K. Rippe, M. Dekker, and N. Kleckner. 2002. Capturing chromosome conformation. *Science*. 295:1306–1311. <https://doi.org/science.1067799>
- Denholtz, M., G. Bonora, C. Chronis, E. Splinter, W. de Laat, J. Ernst, M. Pellegrini, and K. Plath. 2013. Long-range chromatin contacts in embryonic stem cells reveal a role for pluripotency factors and polycomb proteins in genome organization. *Cell Stem Cell*. 13:602–616. <https://doi.org/10.1016/j.stem.2013.08.013>
- Du, Z., L. Jia, Y. Wang, C. Wang, X. Wen, J. Chen, Y. Zhu, D. Yu, L. Zhou, N. Chen, et al. 2018. Combined RNA-seq and RAT-seq mapping of long noncoding RNAs in pluripotent reprogramming. *Sci. Data*. 5:180255. <https://doi.org/10.1038/sdata.2018.255>
- Du, Z., X. Wen, Y. Wang, L. Jia, S. Zhang, Y. Liu, L. Zhou, H. Li, W. Yang, C. Wang, et al. 2021. Author Correction: chromatin lncRNA Platr10 controls stem cell pluripotency by coordinating an intrachromosomal regulatory network. *Genome Biol.* 22:272. <https://doi.org/10.1186/s13059-021-02487-9>
- Fico, A., A. Fiorenzano, E. Pascale, E.J. Patriarca, and G. Minchiotti. 2019. Long non-coding RNA in stem cell pluripotency and lineage commitment: functions and evolutionary conservation. *Cell. Mol. Life Sci.* 76: 1459–1471. <https://doi.org/10.1007/s00018-018-3000-z>
- He, S., H. Zhang, H. Liu, and H. Zhu. 2015. LongTarget: a tool to predict lncRNA DNA-binding motifs and binding sites via Hoogsteen base-pairing analysis. *Bioinformatics*. 31:178–186. <https://doi.org/10.1093/bioinformatics/btu643>
- Huang, H., J. Sun, Y. Sun, C. Wang, S. Gao, W. Li, and J.F. Hu. 2019. Long noncoding RNAs and their epigenetic function in hematological diseases. *Hematol. Oncol.* 37:15–21. <https://doi.org/10.1002/hon.2534>
- Jae, N., A.W. Heumuller, Y. Fouani, and S. Dimmeler. 2019. Long non-coding RNAs in vascular biology and disease. *Vascul. Pharmacol.* 114:13–22. <https://doi.org/10.1016/j.vph.2018.03.003>
- Ji, X., D.B. Dadon, B.E. Powell, Z.P. Fan, D. Borges-Rivera, S. Shachar, A.S. Weintraub, D. Hnisz, G. Pegoraro, T.I. Lee, et al. 2016. 3D chromosome regulatory landscape of human pluripotent cells. *Cell Stem Cell*. 18: 262–275. <https://doi.org/10.1016/j.stem.2015.11.007>
- Kalkan, T., and A. Smith. 2014. Mapping the route from naive pluripotency to lineage specification. *Philos. Trans. R. Soc. Lond. B Biol. Sci.* 369: 20130540. <https://doi.org/10.1098/rstb.2013.0540>
- Kleger, A., P.U. Mahaddalkar, S.F. Katz, A. Lechel, J.Y. Joo, K. Loya, Q. Lin, D. Hartmann, S. Liebau, J.M. Kraus, et al. 2012. Increased reprogramming capacity of mouse liver progenitor cells, compared with differentiated liver cells, requires the BAF complex. *Gastroenterology*. 142:907–917. <https://doi.org/10.1053/j.gastro.2012.01.004>
- Kopp, F. 2019. Molecular functions and biological roles of long non-coding RNAs in human physiology and disease. *J. Gene Med.* 21:e3104. <https://doi.org/10.1002/jgm.3104>
- Krishnan, J., and R.K. Mishra. 2014. Emerging trends of long non-coding RNAs in gene activation. *FEBS J.* 281:34–45. <https://doi.org/10.1111/febs.12578>
- Li, M., and J.C. Izpisua Belmonte. 2018. Deconstructing the pluripotency gene regulatory network. *Nat. Cell Biol.* 20:382–392. <https://doi.org/10.1038/s41556-018-0067-6>
- Li, T., J.F. Hu, X. Qiu, J. Ling, H. Chen, S. Wang, A. Hou, T.H. Vu, and A.R. Hoffman. 2008. CTCF regulates allelic expression of Igf2 by orchestrating a promoter-polycomb repressive complex-2 intrachromosomal loop. *Mol. Cell Biol.* 28:6473–6482. <https://doi.org/10.1128/MCB.00204-08>
- Li, T., H. Chen, W. Li, J. Cui, G. Wang, X. Hu, A.R. Hoffman, and J. Hu. 2014. Promoter histone H3K27 methylation in the control of IGf2 imprinting in human tumor cell lines. *Hum. Mol. Genet.* 23:117–128. <https://doi.org/10.1093/hmg/ddt405>
- Ma, A.N., H. Wang, R. Guo, Y.X. Wang, W. Li, J. Cui, G. Wang, A.R. Hoffman, and J.F. Hu. 2014. Targeted gene suppression by inducing de novo DNA methylation in the gene promoter. *Epigenetics Chromatin*. 7:20. <https://doi.org/10.1186/1756-8935-7-20>
- Mirzadeh Azad, F., I.L. Polignano, V. Proserpio, and S. Oliviero. 2021. Long noncoding RNAs in human stemness and differentiation. *Trends Cell Biol.* 31:542–555. <https://doi.org/10.1016/j.tcb.2021.02.002>
- Morgan, S.L., N.C. Mariano, A. Bermudez, N.L. Arruda, F. Wu, Y. Luo, G. Shankar, L. Jia, H. Chen, J.F. Hu, et al. 2017. Manipulation of nuclear architecture through CRISPR-mediated chromosomal looping. *Nat. Commun.* 8:15993. <https://doi.org/10.1038/ncomms15993>
- Nichols, J., and A. Smith. 2009. Naive and primed pluripotent states. *Cell Stem Cell*. 4:487–492. <https://doi.org/10.1016/j.stem.2009.05.015>
- Niwa, H. 2018. The principles that govern transcription factor network functions in stem cells. *Development*. 145:dev157420. <https://doi.org/10.1242/dev.157420>
- Panepucci, R.A., and I.M. de Souza Lima. 2019. Arrayed functional genetic screenings in pluripotency reprogramming and differentiation. *Stem Cell Res. Ther.* 10:24. <https://doi.org/10.1186/s13287-018-1124-6>
- Papp, B., and K. Plath. 2011. Reprogramming to pluripotency: stepwise resetting of the epigenetic landscape. *Cell Res.* 21:486–501. <https://doi.org/10.1038/cr.2011.28>
- Papp, B., and K. Plath. 2013. Epigenetics of reprogramming to induced pluripotency. *Cell*. 152:1324–1343. <https://doi.org/10.1016/j.cell.2013.02.043>
- Perry, R.B., and I. Ulitsky. 2016. The functions of long noncoding RNAs in development and stem cells. *Development*. 143:3882–3894. <https://doi.org/10.1242/dev.140962>
- Ramazzotti, G., S. Ratti, R. Fiume, M. Yung Follo, A.M. Billi, I. Rusciano, E. Owusu Obeng, L. Manzoli, L. Cocco, and I. Faenza. 2019. Phosphoinositide 3 kinase signaling in human stemcells from reprogramming to differentiation: a talein cytoplasmic and nuclear compartments. *Int. J. Mol. Sci.* 20:2026. <https://doi.org/10.3390/ijms20082026>
- Rasmussen, M.L., N.A. Ortolano, A.I. Romero-Morales, and V. Gama. 2018. Wnt signaling and its impact on mitochondrial and cell cycle dynamics in pluripotent stem cells. *Genes (Basel)*. 9:109. <https://doi.org/10.3390/genes9020109>
- Schulz, S., and S. Haussler. 2014. Chromatin immunoprecipitation for ChIP-chip and ChIP-seq. *Methods Mol. Biol.* 1149:591–605. https://doi.org/10.1007/978-1-4939-0473-0_45
- Sexton, T., and G. Cavalli. 2013. The 3D genome shapes up for pluripotency. *Cell Stem Cell*. 13:3–4. <https://doi.org/10.1016/j.stem.2013.06.013>
- Shiozawa, S., M. Nakajima, J. Okahara, Y. Kuortaki, F. Kisa, S. Yoshimatsu, M. Nakamura, I. Koya, M. Yoshimura, Y. Sasagawa, et al. 2020. Primed to naive-like conversion of the common marmoset embryonic stem cells. *Stem Cells Dev.* 29:761–773. <https://doi.org/10.1089/scd.2019.0259>
- Silva, T.P., J.P. Cotovio, E. Bekman, M. Carmo-Fonseca, J.M.S. Cabral, and T.G. Fernandes. 2019. Design principles for pluripotent stem cell-derived organoid engineering. *Stem Cells Int.* 2019:4508470. <https://doi.org/10.1155/2019/4508470>
- Sun, J., W. Li, Y. Sun, D. Yu, X. Wen, H. Wang, J. Cui, G. Wang, A.R. Hoffman, and J.F. Hu. 2014. A novel antisense long noncoding RNA within the IGfR gene locus is imprinted in hematopoietic malignancies. *Nucleic Acids Res.* 42:9588–9601. <https://doi.org/10.1093/nar/gku549>
- Tosolini, M., and A. Jouneau. 2016. From naive to primed pluripotency: in vitro conversion of mouse embryonic stem cells in epiblast stem cells. *Methods Mol. Biol.* 1341:209–216. https://doi.org/10.1007/7651_2015_208
- Wang, H., W. Li, R. Guo, J. Sun, J. Cui, G. Wang, A.R. Hoffman, and J.F. Hu. 2014. An intragenic long noncoding RNA interacts epigenetically with the RUNX1 promoter and enhancer chromatin DNA in hematopoietic malignancies. *Int. J. Cancer*. 135:2783–2794. <https://doi.org/10.1002/ijc.28922>
- Wang, J., H. Yu, Q. Ma, P. Zeng, D. Wu, Y. Hou, X. Liu, L. Jia, J. Sun, Y. Chen, et al. 2021. Phase separation of OCT4 controls TAD reorganization to promote cell fate transitions. *Cell Stem Cell*. 28:1868–1883.e11. <https://doi.org/10.1016/j.stem.2021.04.023>
- Weinberger, L., M. Ayyash, N. Novershtern, and J.H. Hanna. 2016. Dynamic stem cell states: naive to primed pluripotency in rodents and humans. *Nat. Rev. Mol. Cell Biol.* 17:155–169. <https://doi.org/10.1038/nrm.2015.28>
- Yilmaz, A., and N. Benvenisty. 2019. Defining human pluripotency. *Cell Stem Cell*. 25:9–22. <https://doi.org/10.1016/j.stem.2019.06.010>
- Zhai, Y., X. Chen, D. Yu, T. Li, J. Cui, G. Wang, J.F. Hu, and W. Li. 2015. Histone deacetylase inhibitor valproic acid promotes the induction of pluripotency in mouse fibroblasts by suppressing reprogramming-induced senescence stress. *Exp. Cell Res.* 337:61–67. <https://doi.org/10.1016/j.yexcr.2015.06.003>
- Zhang, H., W. Jiao, L. Sun, J. Fan, M. Chen, H. Wang, X. Xu, A. Shen, T. Li, B. Niu, et al. 2013. Intrachromosomal looping is required for activation of endogenous pluripotency genes during reprogramming. *Cell Stem Cell*. 13:30–35. <https://doi.org/10.1016/j.stem.2013.05.012>
- Zhang, S., Y. Wang, L. Jia, Z. Du, X. Wen, C. Wang, Y. Hao, D. Yu, L. Zhou, N. Chen, et al. 2019. Profiling the long noncoding RNA interaction network

- in the regulatory elements of target genes by chromatin in situ reverse transcription sequencing. *Genome Res.* 29:1521–1532. <https://doi.org/10.1101/gr.244996.118>
- Zhang, S., B. Zhong, M. Chen, G. Yang, Y. Li, H. Wang, G. Wang, W. Li, J. Cui, A.R. Hoffman, and J. Hu. 2014a. Epigenetic reprogramming reverses the malignant epigenotype of the MMP/TIMP axis genes in tumor cells. *Int. J. Cancer.* 134:1583–1594. <https://doi.org/10.1002/ijc.28487>
- Zhang, Z.H., B. Niu, M.J. Zeitz, S. Ge, G. Qian, M.J. Higgins, A.R. Hoffman, and J.F. Hu. 2014b. Long non-coding RNA Kcnqlot1 regulates Kcnq1 imprinting by building a long-range intra-chromosomal loop. *J. Cell. Biol.* 204:61–75. <https://doi.org/10.1083/jcb.201304152>
- Zhao, X., X. Liu, G. Wang, X. Wen, X. Zhang, A.R. Hoffman, W. Li, J.F. Hu, and J. Cui. 2016. Loss of insulin-like growth factor II imprinting is a hallmark associated with enhanced chemo/radiotherapy resistance in cancer stem cells. *Oncotarget.* 7:51349–51364. <https://doi.org/10.18632/oncotarget.9784>
- Zhu, Y., Z. Yan, Z. Du, S. Zhang, C. Fu, Y. Meng, X. Wen, Y. Wang, A.R. Hoffman, J.F. Hu, et al. 2020a. Osblr8 orchestrates intrachromosomal loop structure required for maintaining stem cell pluripotency. *Int. J. Biol. Sci.* 16:1861–1875. <https://doi.org/10.7150/ijbs.45112>
- Zhu, Y., Z. Yan, Z. Tang, and W. Li. 2020b. Novel approaches to profile functional long noncoding RNAs associated with stem cell pluripotency. *Curr. Genomics.* 21:37–45. <https://doi.org/10.2174/1389202921666200210142840>

Supplemental material

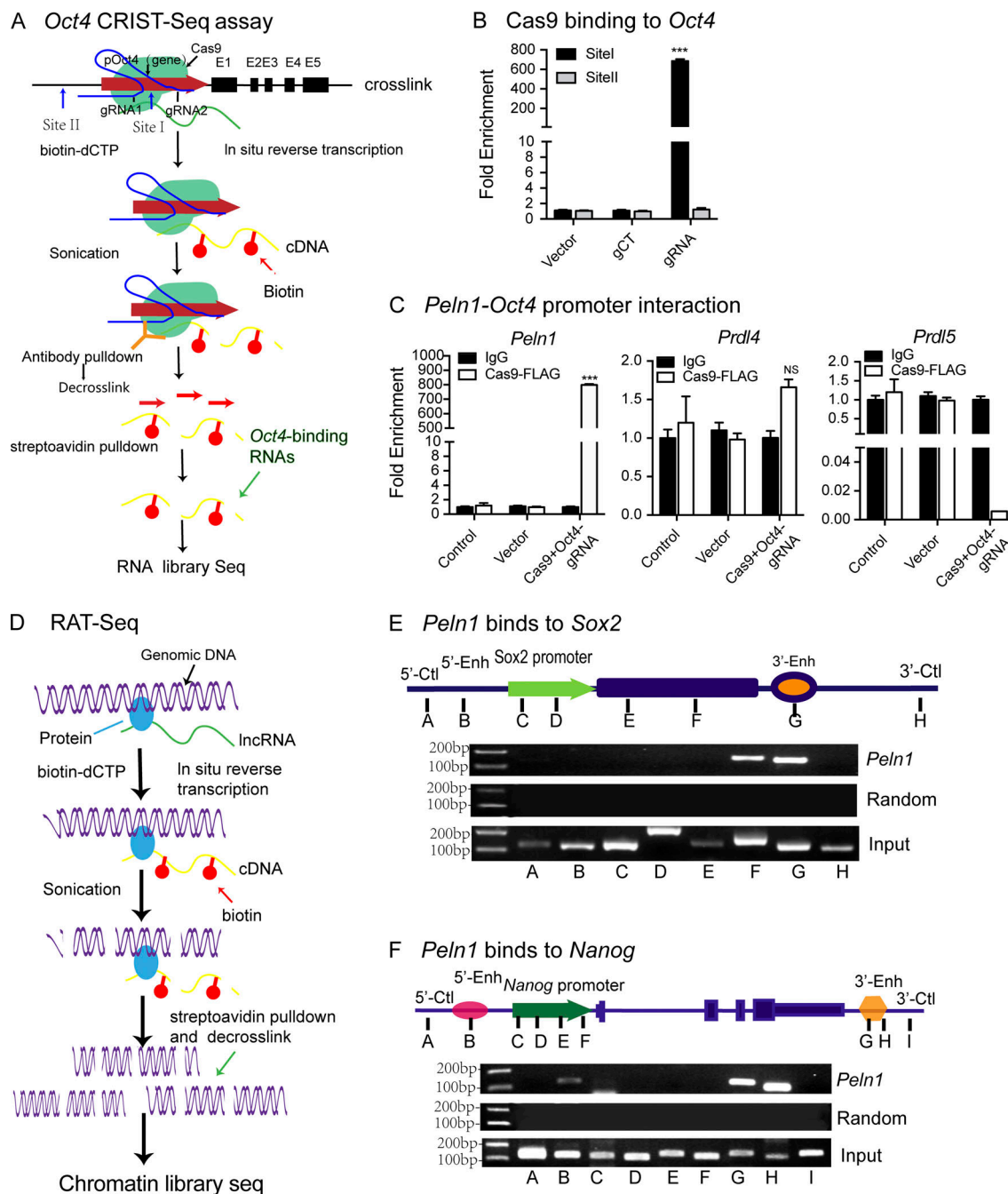


Figure S1. Identification of pluripotency exit-associated lncRNAs by CRIST-seq. (A) Schematic diagram of the CRIST-seq assay. Cas9 *Oct4* gRNA-expressing fibroblasts are cross-linked by formaldehyde and the promoter-interacting RNAs are in situ reverse transcribed into cDNAs with biotin-dCTP in the nucleus. The promoter-interacting cDNAs are isolated by Cas9 immunoprecipitation and streptavidin beads for library sequencing to identify the lncRNAs that interact with the *Oct4* promoter. (B) Specific binding of Cas9 *Oct4* gRNA. Fibroblasts were transfected with the lentiviruses carrying the Cas9 *Oct4*-gRNA, Cas9-gCT (random gRNA), and empty Cas9 vector. After Cas9 immunoprecipitation, the captured DNAs were used for Q-PCR of the *Oct4* targeting site. Data are presented as mean \pm SD of three independent experiments. ***, $P < 0.001$ compared with the controls. Note the specific enrichment of the *Oct4* promoter in the Cas9 *Oct4*-gRNA group. (C) *Pel*1 binding in the CRIST-seq library products. Q-PCR was used to examine the binding of *Pel*1 in the CRIST-seq library products prepared from cells that were transfected with the lentiviruses carrying the Cas9 *Oct4*-gRNA, Cas9 gCT, and Cas9 vector. Cas9-FLAG: the anti-FLAG antibody precipitation for CRIST-seq; IgG: the anti-IgG antibody precipitation as the CRIST control; *Prdl*4-*Prdl*5: pluripotent reprogramming-downregulated lncRNA 4, 5. The data are presented as mean \pm SD of three independent experiments. ***, $P < 0.001$; NS, not significant as compared with the Vector control group. Note the enrichment of *Pel*1 in the Cas9 *Oct4*-gRNA CRIST product as compared with the Cas9 gCT and empty vector controls. No enrichment was detected for two control lncRNAs *Prdl*4 and *Prdl*5. (D) Schematic diagram of RAT-seq. Fibroblasts are cross-linked to fix the RNA-chromatin structure, and chromatin RNAs are reverse transcribed in situ using three *Pel*1-specific complementary primers containing biotin-dCTP. The *Pel*1 cDNA-interacting chromatin complex is pulled down with streptavidin beads and the target gene DNAs are purified for library sequencing. (E) *Pel*1 binding at the *Sox2* locus. A-H: location of PCR primers used to detect the interaction between *Pel*1 and *Sox2*. 5'-Ctl: 5'-Control; 3'-Ctl: 3'-Control; 5'-Enh: 5'-Enhancer; 3'-Enh: 3'-Enhancer. (F) *Pel*1 binding at the *Nanog* gene locus. A-I: location of PCR primers used to detect the interaction between *Pel*1 and *Nanog*.

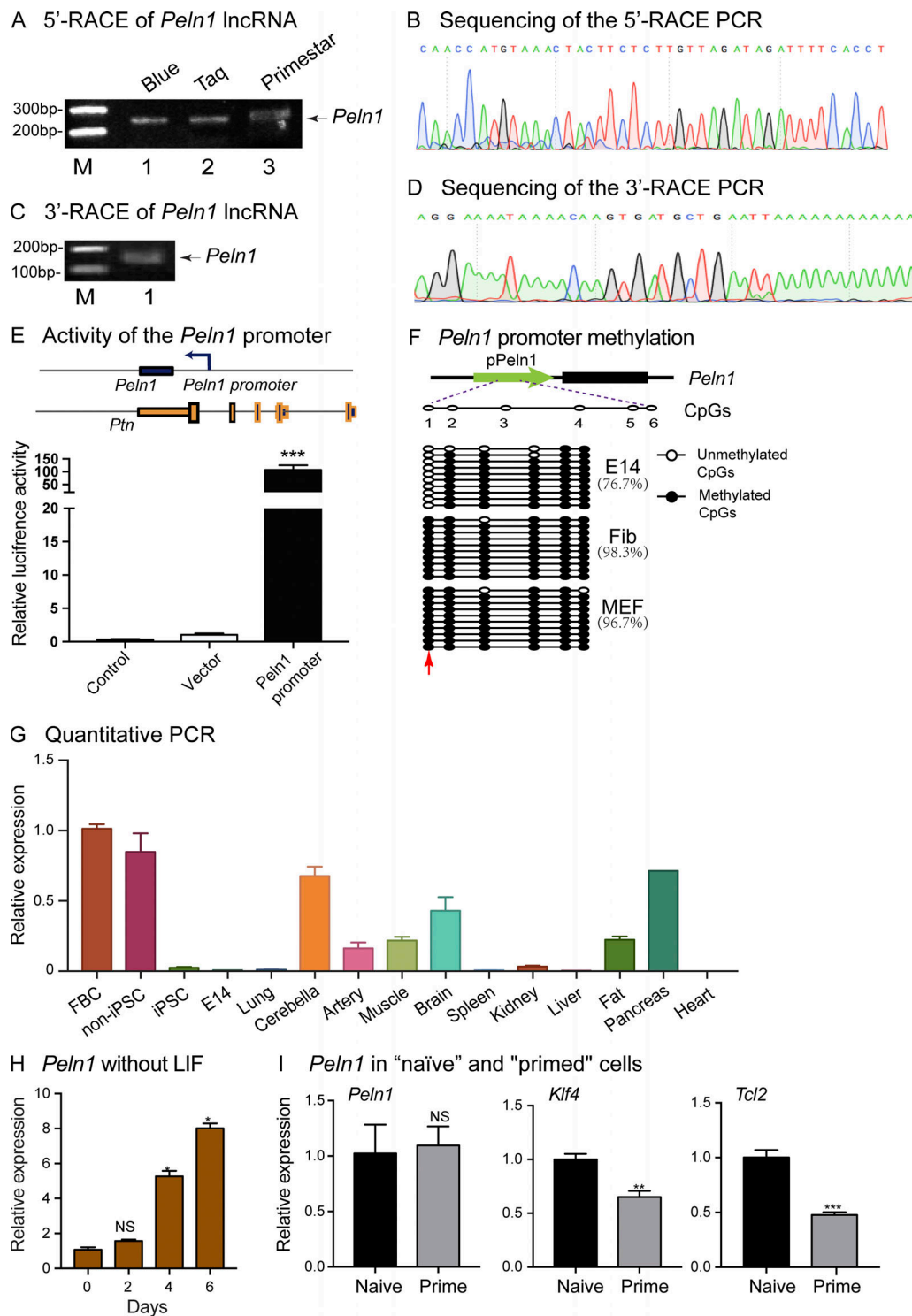


Figure S2. **The *Peln1* promoter and *Peln1* tissue expression.** (A) *Peln1* 5'-RACE: Three PCR enzymes (Blue, Taq, and primestart) were used to amplify the 5'-RACE products. M: 100 bp marker. (B) Sequencing of the 5'-RACE PCR products. (C) *Peln1* 3'-RACE: M-marker. (D) Sequencing of the 3'-RACE PCR. (E) Activity of the *Peln1* promoter. The upstream 2 kb region of *Peln1* was cloned into a pGL3 luciferase plasmid (pGL3-*Peln1* promoter) for the luciferase assay. The pGL3-Basic vector and untreated control cells were used as the controls. The data are presented as mean \pm SD of three independent experiments. ***, $P < 0.001$ as compared with the Vector control group. (F) DNA methylation in the *Peln1* promoter. Sodium bisulfite sequencing was used to compare CpG methylation between E14 cells, fibroblasts, and MEFs at the *Peln1* promoter. Red arrow: the CpG site that shows different methylation. (G) Q-PCR analyses of *Peln1* expression in tissues and cell lines. The data are presented as mean \pm SD of three independent experiments. (H) Expression of *Peln1* in E14 cells following LIF withdrawal. E14 Cells were collected at different stages following LIF withdrawal for Q-PCR quantitation. Data are presented as mean \pm SD of three independent experiments. *, $P < 0.05$; NS, not significant compared with Day 0. (I) *Peln1* expression in "naïve" and "primed" pluripotent cells. Naïve and primed cells were collected for *Peln1* quantitation. *Klf4* and *Tcl2* was used as the positive makers of the "naïve" cells. Data are presented as mean \pm SD of three independent experiments. ***, $P < 0.001$; **, $P < 0.01$; NS, not significant compared with the Naïve group.

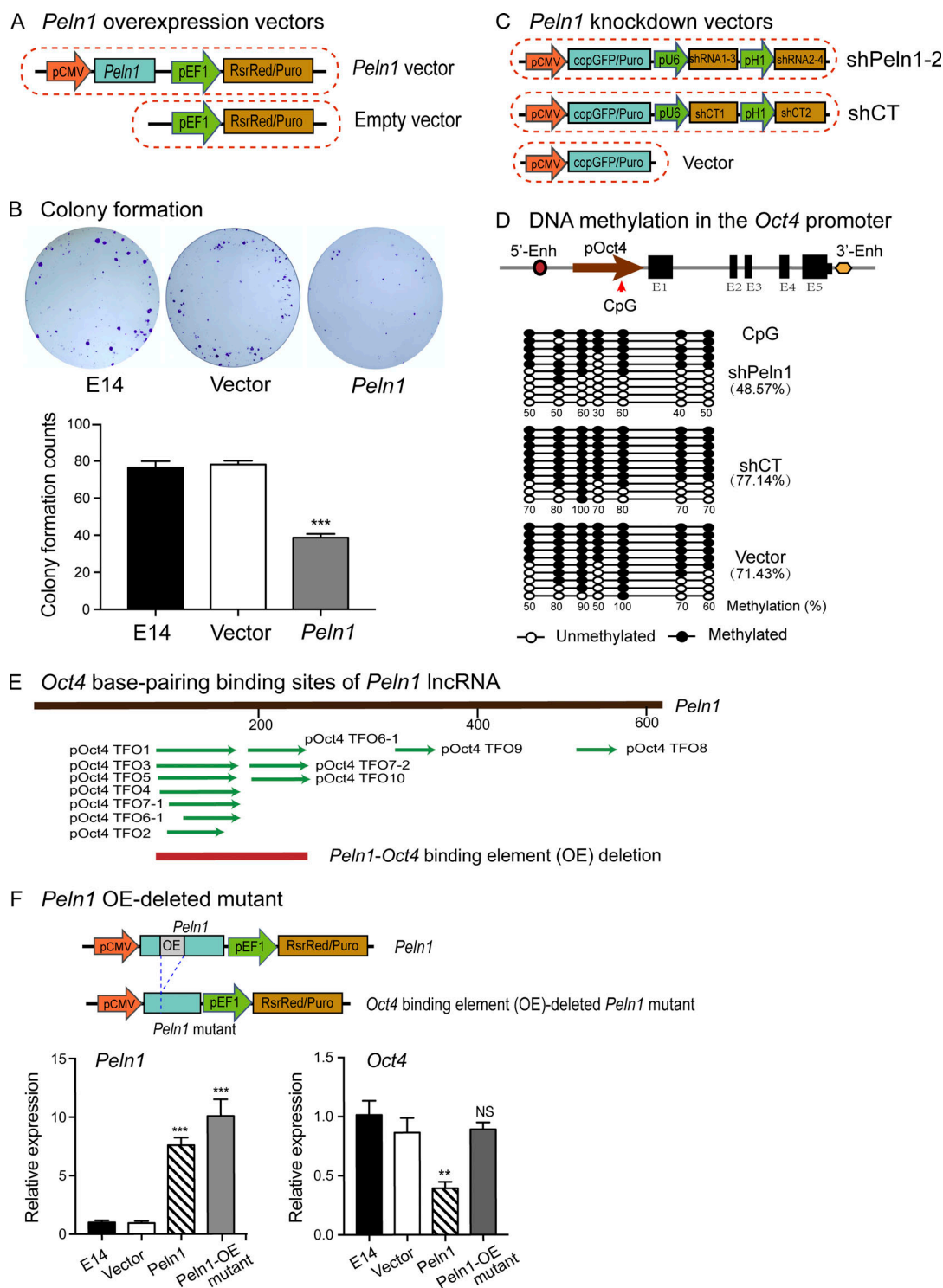


Figure S3. ***Pel*1 in *Oct*4 promoter methylation and colony formation.** (A) Schematic diagrams of plasmid constructs for *Pel*1 overexpression vectors. The empty lentiviral vector was used as the control. (B) Colony formation assays to assess stem cell self-renewal capacity in *Pel*1 overexpressing (OE) and control E14 cells. The data are presented as mean \pm SD of three independent experiments. ***, $P < 0.001$ compared with the Vector and E14 controls. (C) Schematic diagrams of plasmid constructs for *Pel*1 shRNA knockdown vectors. (D) DNA methylation in the *Oct*4 promoter. After *Pel*1 Knockdown in MEFs, sodium bisulfite sequencing was used to compare CpG methylation in the *Oct*4 promoter. sh*Pel*1: sh*Pel*1-knockdown MEFs; shCT: control shRNA MEFs; Vector: lentiviral vector control. Empty circles: unmethylated CpGs; Solid circles: methylated CpGs. (E) Predicted *Oct*4 base-pairing binding sites of *Pel*1 lncRNA. The Hoogsteen base-pairing binding between the *Pel*1 lncRNA and the *Oct*4 DNA was predicted using lncRNA-DNA interaction prediction software (He et al., 2015). TFO1-10: location of predicted *Oct*4 base-pairing sites. (F) *Pel*1 mutant lacks its epigenetic role in regulating *Oct*4 expression. Left panel: *Pel*1 expression. Right panel: *Oct*4 expression. *Pel*1-OE mutant: the *Pel*1 mutant that lacks a 95 bp fragment containing the putative base-pairing region (OE, top panel); *Pel*1: the wild type *Pel*1; Vector: empty vector control. The data are presented as mean \pm SD of three independent experiments. ***, $P < 0.001$; **, $P < 0.01$; NS, not significant compared with the Vector and E14 controls.

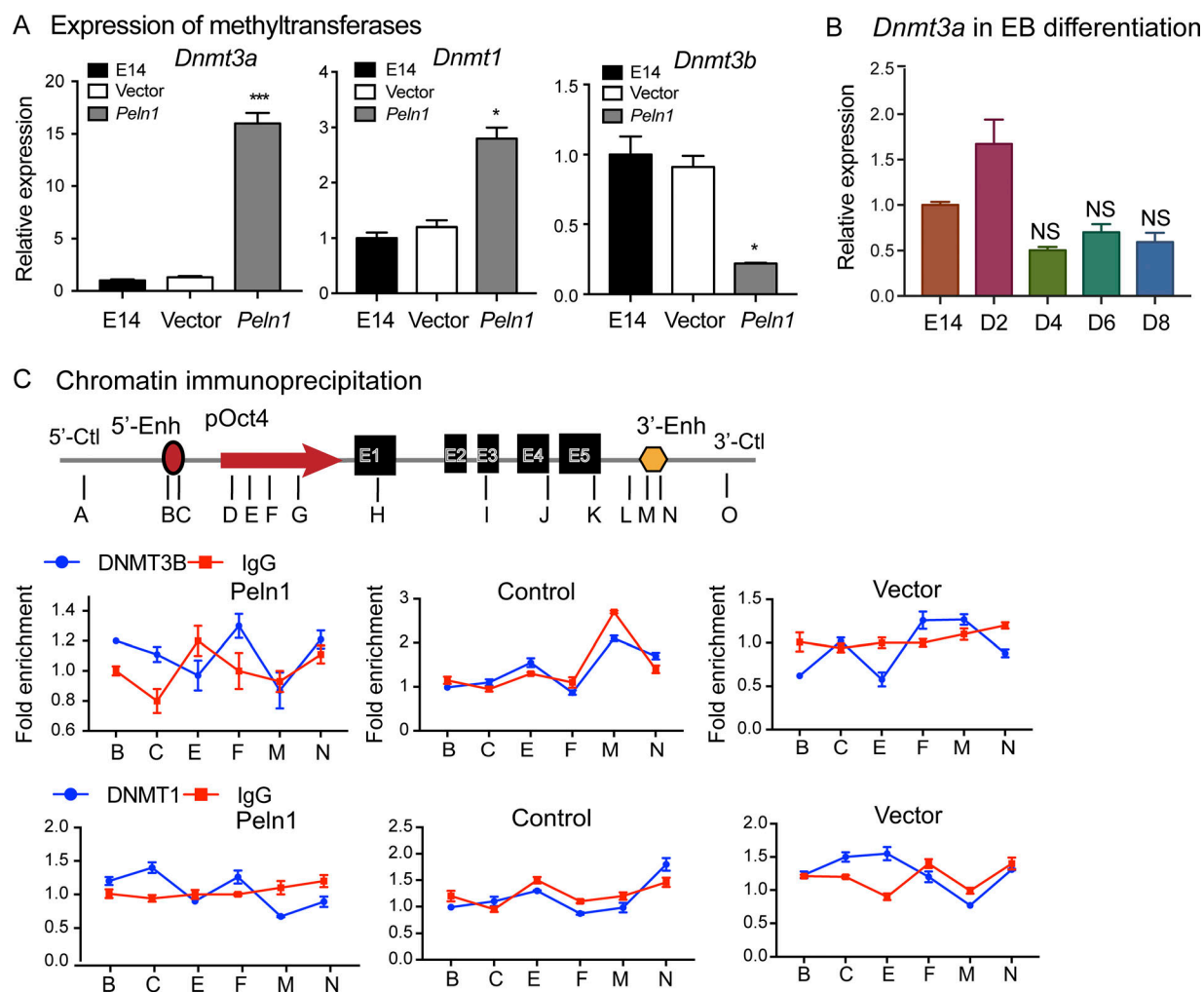
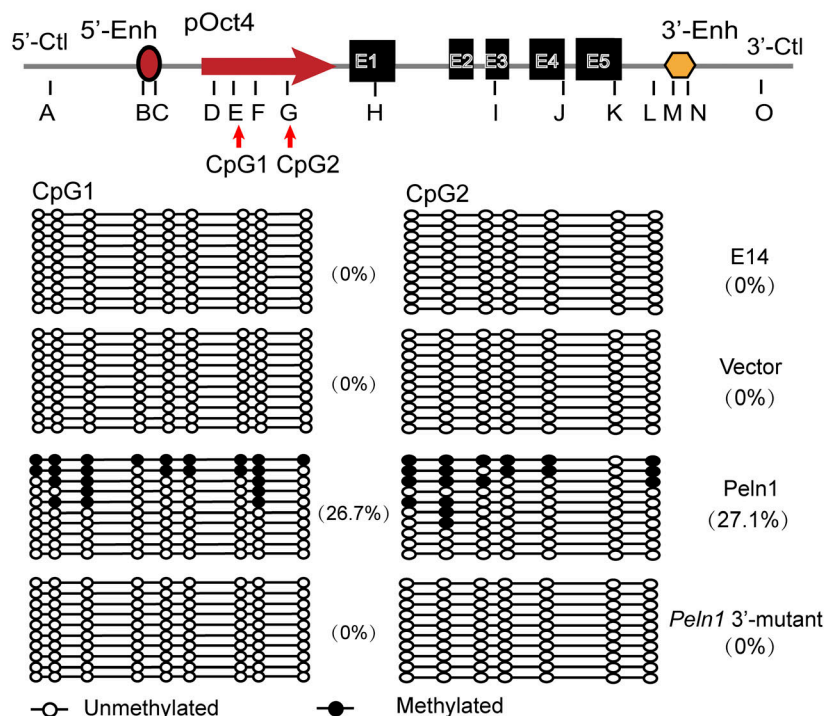


Figure S4. DNA methyltransferase expression and ChIP-Oct4 assay. (A) Quantitation of Dnmt3a, Dnmt3b, and Dnmt1 expression in Peln1-overexpressing E14 cells. Data are presented as mean \pm SD of three independent experiments. ***, $P < 0.001$; *, $P < 0.05$ as compared with the Vector control group. (B) Expression of Dnmt3a in EB differentiation. Cells were collected different stages of EB formation for Q-PCR. Data are presented as mean \pm SD of three independent experiments. NS, not significant compared with the E14 control (Day 0). (C) No DNMT3b and DNMT1 binding to the Oct4 promoter. E14 cells were transfected with lentiviruses carrying the *Peln1* lncRNA, the lncRNA control, and the empty vector. Cells were collected for chromatin immunoprecipitation with anti-DNMT3b, anti-DNMT1, and anti-IgG antibodies. DNMT3b-Oct4 and DNMT1-Oct4 binding was compared between the treatment groups by Q-PCR. Data are presented as mean \pm SD of three independent experiments.

A *Peln1* 3'-mutant and *Oct4* DNA methylation



B *Peln1* 3'-mutant and DNMT3A recruitment

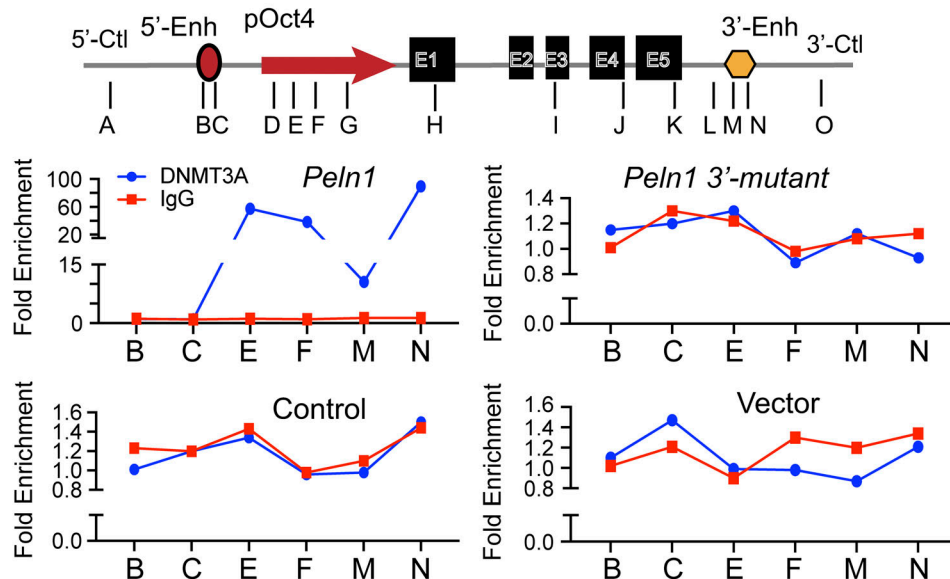


Figure S5. **The *Peln1* 3'-mutant failed to induce DNA methylation in the *Oct4* promoter.** (A) *Peln1* 3'-mutant and *Oct4* DNA methylation. Top panel: location of CpG islands in the *Oct4* locus. Enh: enhancers; pOct4: *Oct4* promoter; E1-E5: *Oct4* exons 1-5; CpG: the cytosine-guanine base pair. Bottom panel: DNA methylation. The *Peln1* 3'-mutant and wild type *Peln1*-overexpressing E14 cells were collected for sodium bisulfite sequencing. Empty circles: unmethylated CpGs; solid circles: methylated CpGs. (B) Lack of DNMT3A recruitment to the *Oct4* locus in *Peln1* 3'-mutant cells. E14 cells transfected with lentiviral WT *Peln1*, *Peln1* 3'-mutant, and the empty vector control were collected for chromatin immunoprecipitation using anti-DNMT3A and anti-IgG antibodies. DNMT3A-*Oct4* binding was compared between treatment groups by Q-PCR. Data are presented as mean \pm SD of three independent experiments. Note the increased binding of DNMT3A to the *Oct4* locus in the *Peln1* cells, but not in the *Peln1* mutant cells.

Provided online is Table S1. Table S1 lists oligonucleotide primers used for PCR.